PREDICTION OF BLAST LOADING AND ITS IMPACT ON BUILDINGS

A THESIS SUBMITTED IN PARTIAL FULFILMENT
OF THE REQUIREMENTS FOR THE DEGREE OF

Master of Technology

in

Civil Engineering

By

NITESH N. MOON

DEPARTMENT OF CIVIL ENGINEERING
NATIONAL INSTITUTE OF TECHNOLOGY
ROURKELA-769008,
2009

PREDICTION OF BLAST LOADING AND ITS IMPACT ON BUILDINGS

A THESIS SUBMITTED IN PARTIAL FULFILMENT

OF THE REQUIREMENTS FOR THE DEGREE OF

Master of Technology
in
Civil Engineering

By

NITESH N. MOON

Under the guidance of

Prof. (Dr.) M. R. BARIK

DEPARTMENT OF CIVIL ENGINEERING
NATIONAL INSTITUTE OF TECHNOLOGY
ROURKELA-769008,

2009

NATIONAL INSTITUTE OF TECHNOLOGY
ROURKELA – 769008, ORISSA
INDIA

CERTIFICATE

This is to certify that the thesis entitled, **"PREDICTION OF BLAST LOADING AND ITS IMPACT ON BUILDINGS"** submitted by **Mr. Nitesh N. Moon** in partial fulfillment of the requirements for the award of **Master of Technology** Degree in **Civil Engineering** with specialization in **Structural Engineering** at the National Institute of Technology, Rourkela is an authentic work carried out by him under my supervision and guidance.

To the best of my knowledge, the matter embodied in this thesis has not been submitted to any other University/ Institute for the award of any degree or diploma.

Dr. M. R. Barik
Dept of Civil Engineering
National Institute of Technology
Rourkela – 769008

Date: 26th May 2009
Place: Rourkela

ACKNOWLEDGEMENT

I wish to express my sincere gratitude to **Prof. M. R. Barik,** for his excellent guidance and perennial encouragement and support during the course of my work in the last one year. I truly appreciate and value his profound knowledge, esteemed supervision and encouragement from the beginning to the end of this thesis.

My special thanks are due to **Prof. M. Panda,** Head of the Civil Engineering Department, for all the facilities provided to successfully complete this work.

I am also very thankful to all the faculty members of the department, especially Structural Engineering specialization for their constant encouragement during the project.

I also take the opportunity to thank all my friends who have directly or indirectly helped me in my project work and in the completion of this report.

Last but not the least I would like to thank my parents, who taught me the value of hard work by their own example. I would like to share this bite of happiness with my mother and father. They rendered me enormous support during the whole tenure of my stay at NIT, Rourkela.

Date: 26th May 2009
Place: Rourkela

Nitesh N. Moon
207CE213
NIT, Rourkela

CONTENTS

			Page No.
ABSTRACT			III
LIST OF FIGURES			IV-VI
LIST OF TABLES			VII
CHAPTER 1		INTRODUCTION	1-2
CHAPTER 2		LITERATURE REVIEW	3-7
	2.1	General	3
	2.2	Objective and Scope of the present work	7
CHAPTER 3		BACKGROUND	8-28
	3.1	Explosion and Blast Phenomenon	8
	3.2	Explosive Air Blast Loading	15
		3.2.1 Blast Waves Scaling Laws	17
		3.2.2 Prediction of Blast Pressure	18
	3.3	Structural Response to Blast Loading	21
		3.3.1 Elastic Single Degree of Freedom (SDOF) System	21
		3.3.2 Elasto-Plastic Single Degree of Freedom (SDOF) System	23
	3.4	Material behavior at High Strain Rate	25
		3.4.1 Dynamic Properties of Concrete Under High-Strain Rates	25
		3.4.2 Dynamic Properties of Reinforcing Steel under High-Strain Rates	27

CHAPTER 4 DYNAMIC LOADING ON STRUCTURE 29-43
4.1 Computation of Dynamic Loading on Closed Rectangular Structures 29
4.1.1 Average Pressure on Front Face 34
4.1.2 Average Pressure on Back Face 35
4.1.3 Average Net Horizontal Pressure 37
4.1.4 Average Pressure on Roof and Sides 38
4.2 Dynamic Loading on Rectangular Structures with Openings 39
4.3 Dynamic Loading on Open-Frame Structures 42
CHAPTER 5 FINITE ELEMENT MODEL 44-54
5.1 Introduction 44
5.2 Structural Nonlinearity 44
5.3 Nonlinearity in Reinforced Cement Concrete 45
5.4 Stress-Strain Curve of Concrete and Steel 46
5.5 Modeling Using ANSYS 49
5.6 Material Model 51
CHAPTER 6 RESULTS AND DISCUSSION 55-62
6.1 RC column subjected to blast loading 55
6.2 Results 60
CHAPTER 7 CONCLUSIONS AND FUTURE NEEDS 63-64
REFERENCES 65-67
APPENDIX 68-76

ABSTRACT

A bomb explosion within or immediately nearby a building can cause catastrophic damage on the building's external and internal structural frames, collapsing of walls, blowing out of large expanses of windows, and shutting down of critical life-safety systems. Loss of life and injuries to occupants can result from many causes, including direct blast-effects, structural collapse, debris impact, fire, and smoke. The indirect effects can combine to inhibit or prevent timely evacuation, thereby contributing to additional casualties.

In addition, major catastrophes resulting from gas-chemical explosions result in large dynamic loads, greater than the original design loads, of many structures. Due to the threat from such extreme loading conditions, efforts have been made during the past three decades to develop methods of structural analysis and design to resist blast loads. Studies were conducted on the behavior of structural concrete subjected to blast loads. These studies gradually enhanced the understanding of the role that structural details play in affecting the behavior.

The response of simple RC columns subjected to constant axial loads and lateral blast loads was examined. The finite element package ANSYS was used to model RC column with different boundary conditions and using the mesh less method to reduce mesh distortions. For the response calculations, a constant axial force was first applied to the column and the equilibrium state was determined. Next, a short duration, lateral blast load was applied and the response time history was calculated.

The analysis and design of structures subjected to blast loads require a detailed understanding of blast phenomena and the dynamic response of various structural elements. This gives a comprehensive overview of the effects of explosion on structures.

LIST OF FIGURES

Figure No.	Title	Page No.
Fig.3.1	(a) Variation of pressure with distance	10
	(b) Formation of shock front in a shock wave	10
	(c) Variation of overpressure with distance from centre of explosion at various times	10
Fig.3.2	(a) The variation of overpressure with distance at a given time from centre of explosion	11
	(b) Variation of overpressure with distance at a time from the explosion	12
	(c) Variation of dynamic pressure with distance at a time from the explosion	12
Fig.3.3	(a) Response of seismic loading on structure	15
	(b) Response of blast loading on structure	15
Fig.3.4	Blast Loads on a Building	17
Fig.3.5	(a) SDOF system	22
	(b) Blast loading	22
Fig.3.6	Simplified resistance function of an elasto-plastic SDOF system	24
Fig.3.7	Maximum response of elasto-plastic SDF system to a triangular load	24
Fig.3.8	Strain rates associated with different types of loading	25
Fig. 3.9	Stress-strain curves of concrete at different strain rates	26
Fig.3.10	Dynamic Increase Factor (DIF) for peak stress of concrete	27
Fig.4.1	Closed rectangular structure	29
Fig.4.2	Positive phase duration of overpressure for surface burst	30
Fig.4.3	Peak overpressure and peak dynamic pressure for surface burst	31
Fig.4.4	Positive phase duration of overpressure and dynamic pressure	32
Fig.4.5	Rate of decay of overpressure for various values of P_{so}	33
Fig.4.6	Rate of decay of dynamic pressure for various values of P_{so}	33

Figure No.	Title	Page No.
Fig.4.7	Average front face pressure verses time	34
Fig. 4.8	Average back face pressure versus time	37
Fig. 4.9	Average net horizontal pressure versus time	37
Fig.4.10	Average side and roof pressure versus time	38
Fig. 4.11	Subdivision of a typical wall with openings	39
Fig.4.12	Time variation of front face average pressure	40
Fig.4.13	Time variations of side and top average pressures	41
Fig.4.14	Time variation of back face average pressure	41
Fig.4.15	Net horizontal loading of an open frame structure	43
Fig.5.1	Stress-strain curves of concrete in compression	47
Fig.5.2	Uniaxial Stress-Strain curves of different steels	48
Fig.5.3	(a) SOLID65 Element	50
	(b) LINK8 Element	51
Fig. 5.4	Idealized elasto-plastic stress-strain curve	52
Fig. 5.5	Multi-linear Isotropic stress-strain curve	54
Fig.6.1	Cross section of the NSC column- ordinary detailing 400 mm stirrups spacing	56
Fig.6.2	Blast loading	56
Fig.6.3	Free-field pressure –time variation for height= 0m	58
Fig.6.4	Free-field pressure –time variation for height = 6.4	59
Fig.6.5	3D model of the column using ANSYS	60
Fig.6.6	Lateral Deflection – Time history at mid point of column with 400 mm stirrups spacing	61
Fig. 6.7	Lateral Deflection – Time history at mid point of column with 100 mm stirrups spacing	61

Figure No.	Title	Page No.
Fig. A1	Positive Phase Shock Wave Parameter for a Spherical TNT Explosion in Free Air	68
Fig. A2	Negative Phase Shock Wave Parameter for a Spherical TNT Explosion in Free Air	69
Fig. A3	Variation of Reflected Pressure as a Function of Angle of Incidence	70
Fig. A4	Variation of Scaled Reflected Impulse as a Function of Incidence	71
Fig. A5	Peak Incident Pressure versus the Ratio of Normal Reflected Pressure/ Incidence Pressure for a Free Air Burst	72
Fig. A6	Peak Incident Pressure versus Peak Dynamic Pressure, Density of Air Behind the Shock Front, and Particle Velocity	73
Fig. A7	Positive Phase Shock Wave Parameters for a Hemispherical TNT Explosion on The surface	74
Fig. A8	3D finite element model of simple RC column in ANSYS	75
Fig. A9	3D finite element model of simple RC column with axial load and blast pressure	76

LIST OF TABLES

Table No.	Title	Page No.
Table 3.1	Peak reflected overpressures *Pr* (in MPa) with different W-R combinations	19
Table 5.1	Stress-strain properties of M 40 concrete using multi crack model	54
Table 6.1	Concrete grades and member size	55
Table 6.2	Comparison of the lateral deflection at mid point of HSC and NSC columns	62

Chapter - 1

INTRODUCTION

Chapter 1

INTRODUCTION

In the past few decades considerable emphasis has been given to problems of blast and earthquake. The earthquake problem is rather old, but most of the knowledge on this subject has been accumulated during the past fifty years. The blast problem is rather new; information about the development in this field is made available mostly through publication of the Army Corps of Engineers, Department of Defense, U.S. Air Force and other governmental office and public institutes. Much of the work is done by the Massachusetts Institute of Technology, The University of Illinois, and other leading educational institutions and engineering firms.

Due to different accidental or intentional events, the behavior of structural components subjected to blast loading has been the subject of considerable research effort in recent years. Conventional structures, particularly that above grade, normally are not designed to resist blast loads; and because the magnitudes of design loads are significantly lower than those produced by most explosions, conventional structures are susceptible to damage from explosions. With this in mind, developers, architects and engineers increasingly are seeking solutions for potential blast situations, to protect building occupants and the structures.

Disasters such as the terrorist bombings of the U.S. embassies in Nairobi, Kenya and Dar es Salaam, Tanzania in 1998, the Khobar Towers military barracks in Dhahran, Saudi Arabia in 1996, the Murrah Federal Building in Oklahoma City in 1995, and the World Trade Center in New York in 1993 have demonstrated the need for a thorough examination of the behavior of columns subjected to blast loads. To provide adequate protection against explosions,

the design and construction of public buildings are receiving renewed attention of structural engineers. Difficulties that arise with the complexity of the problem, which involves time dependent finite deformations, high strain rates, and non-linear inelastic material behavior, have motivated various assumptions and approximations to simplify the models. These models span the full range of sophistication from single degree of freedom systems to general purpose finite element programs such as ABAQUS, ANSYS, and ADINA etc. [1].

Chapter – 2

LITERATURE REVIEW OBJECTIVE AND SCOPE OF STUDY

Chapter 2

REVIEW OF LITERATURE

2.1 GENERAL

The analysis of the blast loading on the structure started in 1960's. US Department of the Army, released a technical manual titled "structures to resist the effects of accidental explosions" in 1959. The revised edition of the manual TM 5-1300 (1990) most widely used by military and civilian organization for designing structures to prevent the propagation of explosion and to provide protection for personnel and valuable equipments.

The methods available for prediction of blast effects on buildings structures are:

- Empirical (or analytical) methods
- Semi-empirical methods
- Numerical methods.

Empirical methods are essentially correlations with experimental data. Most of these approaches are limited by the extent of the underlying experimental database. The accuracy of all empirical equations diminishes as the explosive event becomes increasingly near field.

Semi-empirical methods are based on simplified models of physical phenomena. The attempt is to model the underlying important physical processes in a simplified way. These methods are dependent on extensive data and case study. The predictive accuracy is generally better than that provided by the empirical methods.

Numerical (or first-principle) methods are based on mathematical equations that describe the basic laws of physics governing a problem. These principles include conservation of mass, momentum, and energy. In addition, the physical behavior of materials is described by

constitutive relationships. These models are commonly termed computational fluid dynamics (CFD) models.

The key elements are the loads produced from explosive sources, how they interact with structures and the way structures respond to them. Explosive sources include gas, high explosives, dust and nuclear materials. The basic features of the explosion and blast wave phenomena are presented along with a discussion of TNT (trinitrotoluene) equivalency and blast scaling laws. The characteristics of incident overpressure loading due to atomic weapons, conventional high explosives and unconfined vapors cloud explosions are addressed and followed by a description of the other blast loading components associated with air flow and reflection process. Fertice G. [8] has extensive study of the structures and computation of blast loading on aboveground structures.

A. Khadid et al. **[1]** studied the fully fixed stiffened plates under the effect of blast loads to determine the dynamic response of the plates with different stiffener configurations and considered the effect of mesh density, time duration and strain rate sensitivity. He used the finite element method and the central difference method for the time integration of the nonlinear equations of motion to obtain numerical solutions.

A.K. Pandey et al. **[2]** studied the effects of an external explosion on the outer reinforced concrete shell of a typical nuclear containment structure. The analysis has been made using appropriate non-linear material models till the ultimate stages. An analytical procedure for non-linear analysis by adopting the above model has been implemented into a finite element code DYNAIB.

Alexander M. Remennikov **[3]** studied the methods for predicting bomb blast effects on buildings. When a single building is subjected to blast loading produced by the detonation of high explosive device. Simplified analytical techniques used for obtaining conservative estimates of the blast effects on buildings. Numerical techniques including Lagrangian, Eulerian, Euler-FCT, ALE, and finite element modelling used for accurate prediction of blast loads on commercial and public buildings.

J. M. Dewey **[11]** studied the properties of the blast waves obtained from the particle trajectories. First time he introduced the effect of spherical and hemispherical TNT (trinitrotoluene) in blast waves and determined the density throughout the flow by application of the Lagrangian conservation of mass equation which used for calculating the pressure by assuming the adiabatic flow for each air element between the shock fronts. The temperature and the sound speed found from the pressure and density, assuming the perfect gas equation of states.

Kirk A. Marchand et al. **[13]** reviews the contents of American Institute of Steel Construction, Inc. for facts for steel buildings give a general science of blast effects with the help of numbers of case studies of the building which are damaged due to the blast loading i.e. Murrah Building, Oklahoma City, Khobar Towers , Dhahran, Saudi Arabia and others. Also studied the dynamic response of a steel structure to the blast loading and shows the behavior of ductile steel column and steel connections for the blast loads.

M. V. Dharaneepathy et al. **[14]** studied the effects of the stand-off distance on tall shells of different heights, carried out with a view to study the effect of distance (ground-zero distance) of charge on the blast response. An important task in blast-resistant design is to make a realistic prediction of the blast pressures. The distance of explosion from the structure is an important datum, governing the magnitude and duration of the blast loads. The distance, known as ‘critical

ground-zero distance', at which the blast response is a maximum. This critical distance should be used as design distance, instead of any other arbitrary distance.

Ronald L. Shope **[16]** studied the response of wide flange steel columns subjected to constant axial load and lateral blast load. The finite element program ABAQUS was used to model with different slenderness ratio and boundary conditions. Non-uniform blast loads were considered. Changes in displacement time histories and plastic hinge formations resulting from varying the axial load were examined.

T. Borvik et al. **[21]** studied the response of a steel container as closed structure under the blast loads. He used the mesh less methods based on the Lagrangian formulations to reduce mesh distortions and numerical advection errors to describe the propagation of blast load. All parts are modelled by shell element type in LS-DYNA. A methodology has been proposed for the creation of inflow properties in uncoupled and fully coupled Eulerian–Lagrangian LS-DYNA simulations of blast loaded structures.

TM 5-1300 (UFC 3-340-02) **[22]** is a manual titled "structures to resist the effects of accidental explosions" which provides guidance to designers, the step-to-step analysis and design procedure, including the information on such items (1) blast, fragment and shock loading. (2) principle on dynamic analysis. (3) reinforced and structural steel design and (4) a number of special design considerations.

T. Ngo, et al.**[23]** for there study on "Blast loading and Blast Effects on Structures" gives an overview on the analysis and design of structures subjected to blast loads phenomenon for understanding the blast loads and dynamic response of various structural elements. This study helps for the design consideration against extreme events such as bomb blast, high velocity impacts.

2.2 OBJECTIVE AND SCOPE OF THE PRESENT WORK

OBJECTIVE:

- For analyse and design the structures against the abnormal loading conditions like blast loads, strong wind pressure etc. requiring detailed understanding of blast phenomenon.
- To study the dynamic response of various structural elements like column, beam, slab and connections in steel and RCC structures.
- The main objective of the research presented in this thesis is to analytically and numerically study the structural behavior of HSC and NSC column subjected to blast loading.

SCOPE OF THE STUDY:

In order to achieve the above-mentioned objectives the following tasks have been carried out:

- All the computation of dynamic loading on a rectangular structure with and without openings and open frame structures to evaluate the blast pressure.
- Computation of the blast loading on the column.
- Modeling of a simple RC column in ANSYS.
- Response of a simple RC column under the Blast loading.

Chapter – 3

BACKGROUND

Chapter 3

BACKGROUND

3.1 EXPLOSION AND BLAST PHENOMENON

In general, an explosion is the result of a very rapid release of large amounts of energy within a limited space. Explosions can be categorized on the basis of their nature as physical, nuclear and chemical events.

In physical explosion: - Energy may be released from the catastrophic failure of a cylinder of a compressed gas, volcanic eruption or even mixing of two liquid at different temperature.

In nuclear explosion: - Energy is released from the formation of different atomic nuclei by the redistribution of the protons and neutrons within the inner acting nuclei.

In chemical explosion: - The rapid oxidation of the fuel elements (carbon and hydrogen atoms) is the main source of energy.

The type of burst mainly classified as

a. Air burst
b. High altitude burst
c. Under water burst
d. Underground burst
e. Surface burst

The discussion in this section is limited to air burst or surface burst. This information is then used to determine the dynamic loads on surface structures that are subjected to such blast pressures and to design them accordingly. It should be pointed out that surface structure cannot

be protected from a direct hit by a nuclear bomb; it can however, be designed to resist the blast pressures when it is located at some distance from the point of burst.

The destructive action of nuclear weapon is much more severe than that of a conventional weapon and is due to blast or shock. In a typical air burst at an altitude below 100,000 ft. an approximate distribution of energy would consist of 50% blast and shock, 35% thermal radiation, 10% residual nuclear radiation and 5% initial nuclear radiation [8].

The sudden release of energy initiates a pressure wave in the surrounding medium, known as a shock wave as shown in Fig.3.1 (a). When an explosion takes place, the expansion of the hot gases produces a pressure wave in the surrounding air. As this wave moves away from the centre of explosion, the inner part moves through the region that was previously compressed and is now heated by the leading part of the wave. As the pressure waves moves with the velocity of sound, the temperature is about 3000^{o}-4000^{o}C and the pressure is nearly 300 kilobar of the air causing this velocity to increase. The inner part of the wave starts to move faster and gradually overtakes the leading part of the waves. After a short period of time the pressure wave front becomes abrupt, thus forming a shock front some what similar to Fig.3.1 (b). The maximum overpressure occurs at the shock front and is called the peak overpressure. Behind the shock front, the overpressure drops very rapidly to about one-half the peak overpressure and remains almost uniform in the central region of the explosion.

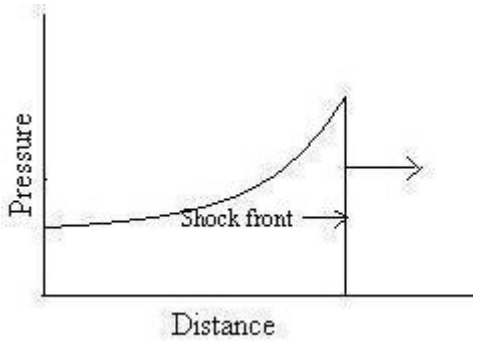

Fig.3.1 (a) Variation of pressure with distance

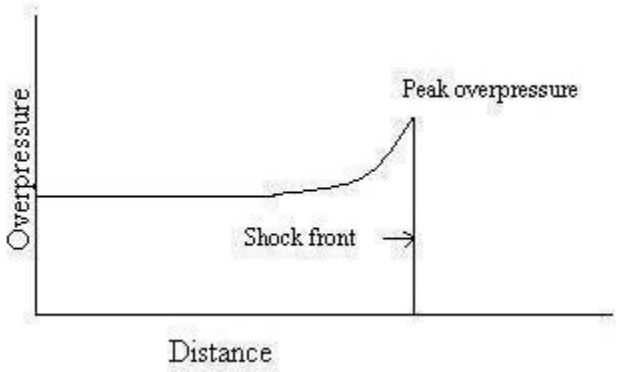

Fig.3.1 (b) Formation of shock front in a shock wave.

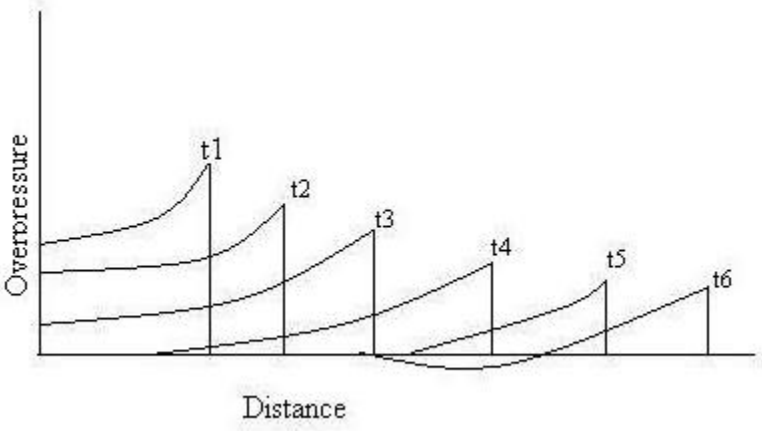

Fig.3.1 (c) Variation of overpressure with distance from centre of explosion at various times.

An expansion proceeds, the overpressure in the shock front decreases steadily; the pressure behind the front does not remain constant, but instead, fall off in a regular manner. After a short time, at a certain distance from the centre of explosion, the pressure behind the shock front becomes smaller than that of the surrounding atmosphere and so called negative-phase or suction.

The front of the blast waves weakens as it progresses outward, and its velocity drops towards the velocity of the sound in the undisturbed atmosphere. This sequence of events is shown in Fig.3.1(c), the overpressure at time t1, t2…..t6 are indicated. In the curves marked t_1 to t_5, the pressure in the blast has not fallen below that of the atmosphere. In the curve t_6 at some distance behind the shock front, the overpressure becomes negative. This is better illustrated in Fig.3.2 (a).

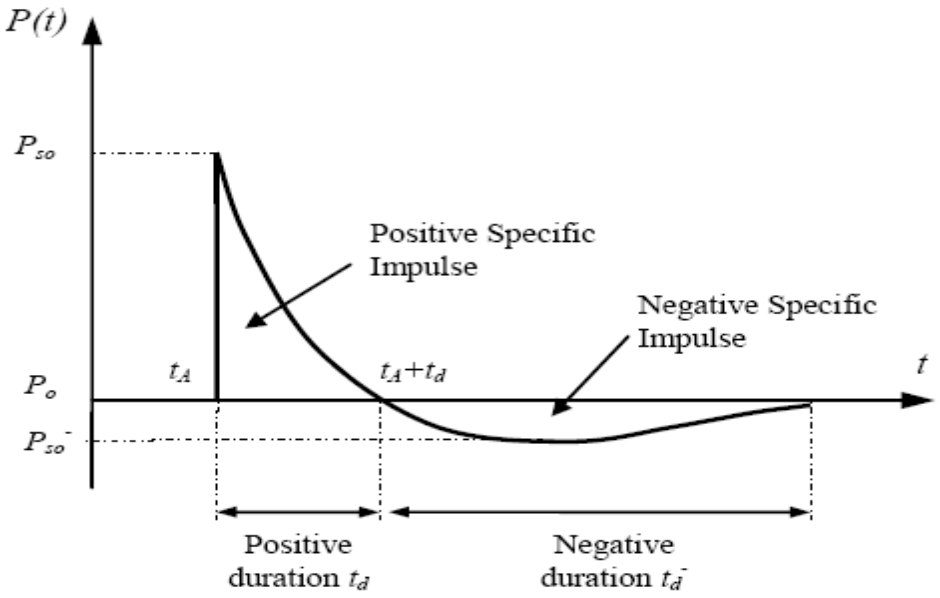

Fig.3.2 (a) The variation of overpressure with distance at a given time from centre of explosion.

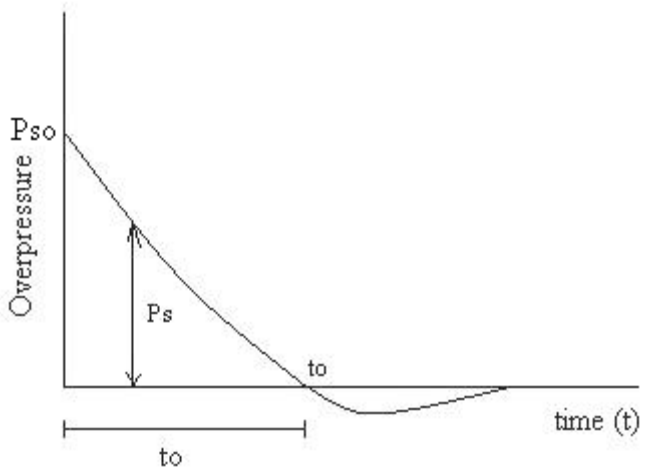

Fig.3.2 (b) Variation of overpressure with distance at a time from the explosion.

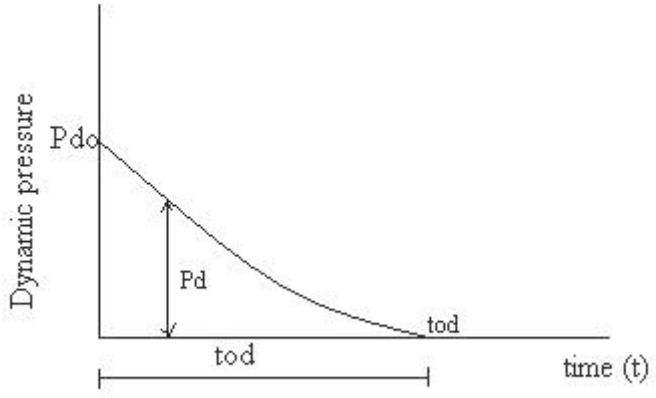

Fig.3.2(c) Variation of dynamic pressure with distance at a time from the explosion.

The time variation of the same blast wave at a given distance from the explosion is shown in Fig 3.2(b); to indicate the time duration of the positive phase and also the time at the end of the positive phase. Another quantity of the equivalent importance is the force that is developed from the strong winds accompanying the blast wave known as the dynamic pressure; this is proportional to the square of the wind velocity and the density of the air behind the shock front. Its variation at a given distance from the explosion is shown in Fig.3.2(c).

Mathematically the dynamic pressure P_d is expressed as.

$$P_d = \frac{1}{2}\rho u^2 \text{.....1}$$

Where u is the velocity of the air particle and
ρ is the air density

The peak dynamic pressure decreases with increasing distance from the centre of explosion, but the rate of decrease is different from that of the peak overpressure. At a given distance from the explosion, the time variation of the dynamic P_d behind the shock front is somewhat similar to that of the overpressure P_s, but the rate of decrease is usually different. For design purposes, the negative phase of the overpressure in Fig.3.2 (b) is not important and can be ignored.

Explosive and impact loads similar to and different from loads typically used in building design.

Explosive loads and impact loads are transients, or loads that are applied dynamically as one-half cycle of high amplitude, short duration air blast or contact and energy transfer related pulse. This transient load is applied only for a specific and typically short period of time in the case of blast loads, typically less than one-tenth of a second [13]. This means that an additional set of dynamic structural properties not typically considered by the designer, such as rate dependant material properties and inertial effects must be considered in design.

Often, design to resist blast, impact and other extraordinary loads must be thought of in the context of life safety, not in terms of serviceability or life-cycle performance. Performance criteria for other critical facilities (nuclear reactors, explosive and impact test facilities, etc.) may require serviceability and reuse, but most commercial office and industrial facilities will not have to perform to these levels. Structures designed to resist the effects of explosions and impact are

permitted to contribute all of their resistance, both material linear and non-linear (elastic and inelastic), to absorb damage locally, so as to not compromise the integrity of the entire structure. It is likely that local failure can and may be designed to occur, due to the uncertainty associated with the loads.

How blast loads are different from seismic loads.

Blast loads are applied over a significantly shorter period of time (orders-of-magnitude shorter) than seismic loads. Thus, material strain rate effects become critical and must be accounted for in predicting connection performance for short duration loadings such as blast. Also, blast loads generally will be applied to a structure non-uniformly, i.e., there will be a variation of load amplitude across the face of the building, and dramatically reduced blast loads on the sides and rear of the building away from the blast. Figure 3.3 shows a general comparison between an acceleration record from a point 7 km from the 1994 Northridge epicenter and the predicted column loads for the 1995 Oklahoma City bombing [13].

It is apparent that the 12-second-long ground shaking from the Northridge event lasted approximately 1000 times longer than the 9 ms initial blast pulse from the Murrah Building blast. The effects of blast loads are generally local, leading to locally severe damage or failure. Conversely, seismic "loads" are ground motions applied uniformly across the base or foundation of a structure. All components in the structure are subjected to the "shaking" associated with this motion.

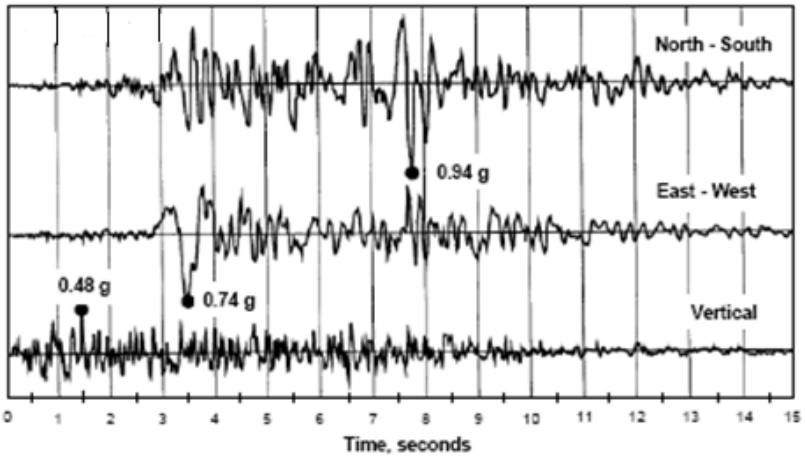

(a) Response of seismic loading on structure.

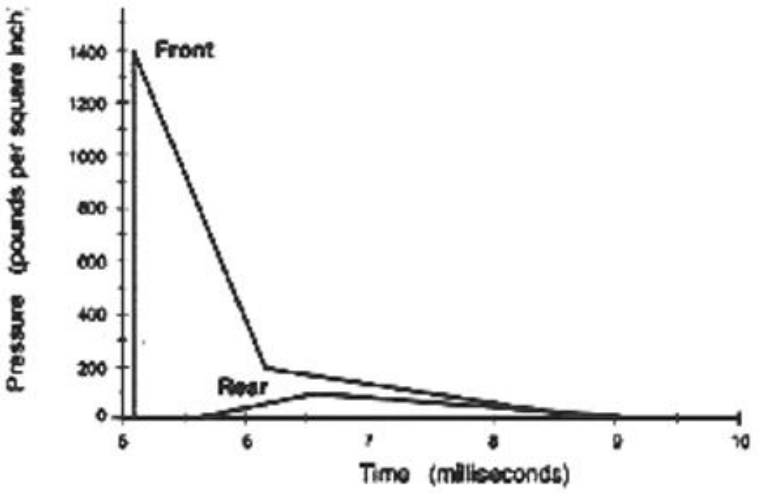

(b) Response of blast loading on structure.

Fig.3.3. Comparison between seismic load and the blast load

3.2 EXPLOSIVE AIR BLAST LOADING

The threat for a conventional bomb is defined by two equally important elements, the bomb size, or charge weight *W*, and the standoff distance (*R)* between the blast source and the target (Fig.3.4). For example, the blast occurred at the basement of World Trade Centre in 1993 has the charge weight of 816.5 kg TNT. The Oklahoma bomb in 1995 has a charge weight of

1814 kg at a stand off of 5m [13]. As terrorist attacks may range from the small letter bomb to the gigantic truck bomb as experienced in Oklahoma City, the mechanics of a conventional explosion and their effects on a target must be addressed.

Throughout the pressure-time profile, two main phases can be observed; portion above ambient is called positive phase of duration (t_d), while that below ambient is called negative phase of duration (t_d). The negative phase is of a longer duration and a lower intensity than the positive duration. As the stand-off distance increases, the duration of the positive-phase blast wave increases resulting in a lower-amplitude, longer-duration shock pulse. Charges situated extremely close to a target structure impose a highly impulsive, high intensity pressure load over a localized region of the structure; charges situated further away produce a lower-intensity, longer-duration uniform pressure distribution over the entire structure. Eventually, the entire structure is engulfed in the shock wave, with reflection and diffraction effects creating focusing and shadow zones in a complex pattern around the structure. During the negative phase, the weakened structure may be subjected to impact by debris that may cause additional damage.

STAND-OFF DISTANCE

Stand-off distance refers to the direct, unobstructed distance between a weapon and its target.

HEIGHT OF BURST (HOB)

Height of burst refers to aerial attacks. It is the direct distance between the exploding weapon in the air and the target.

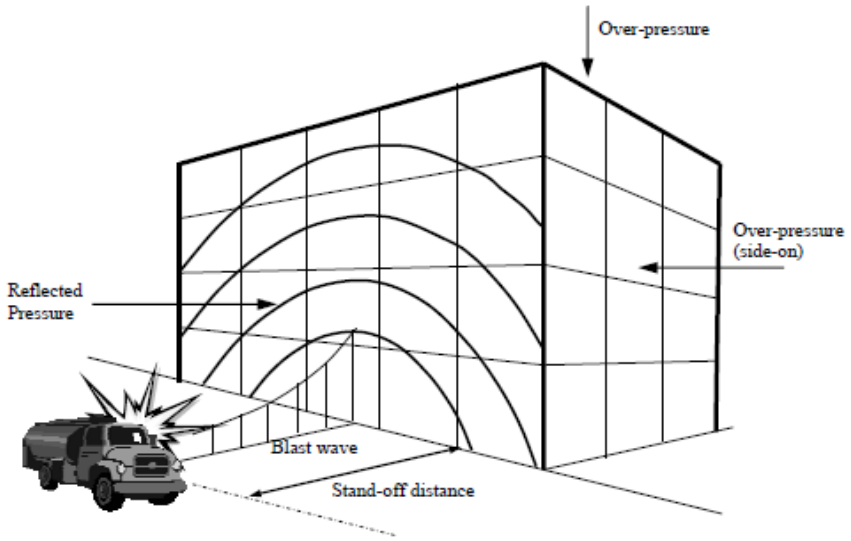

Figure 3.4: Blast Loads on a Building.

If the exterior building walls are capable of resisting the blast load, the shock front penetrates through window and door openings, subjecting the floors, ceilings, walls, contents, and people to sudden pressures and fragments from shattered windows, doors, etc. Building components not capable of resisting the blast wave will fracture and be further fragmented and moved by the dynamic pressure that immediately follows the shock front. Building contents and people will be displaced and tumbled in the direction of blast wave propagation. In this manner the blast will propagate through the building.

3.2.1 BLAST WAVE SCALING LAWS

All blast parameters are primarily dependent on the amount of energy released by a detonation in the form of a blast wave and the distance from the explosion. A universal normalized description of the blast effects can be given by scaling distance relative to $(E/P\text{o})^{1/3}$ and scaling pressure relative to $P\text{o}$, where E is the energy release (kJ) and $P\text{o}$ the ambient

pressure (typically 100 kN/m2). For convenience, however, it is general practice to express the basic explosive input or charge weight W as an equivalent mass of TNT. Results are then given as a function of the dimensional distance parameter,

$$\text{Scaled Distance}(Z) = \frac{R}{W^{1/3}} \qquad \ldots\ldots\ldots\ldots\ldots 2$$

Where R is the actual effective distance from the explosion.
W is generally expressed in kilograms.

Scaling laws provide parametric correlations between a particular explosion and a standard charge of the same substance.

3.2.2 PREDICTION OF BLAST PRESSURE

Blast wave parameter for conventional high explosive materials have been the focus of a number of studies during the 1950's and 1960's.

The estimations of peak overpressure due to spherical blast based on scaled distance $Z=R/W^{1/3}$ was introduced by Brode (1955) as:

$$P_{so} = \frac{6.7}{Z^3} + 1 \text{ bar} \quad (P_{so} > 10\text{bar}) \qquad \ldots\ldots\ldots\ldots\ldots\ldots\ldots (3.a)$$

$$P_{so} = \frac{0.975}{Z} + \frac{1.455}{Z^2} + \frac{5.85}{Z^3} - 0.019 \text{ bar} \quad (0.1 < P_{so} < 10 \text{ bar}) \quad \ldots\ldots\ldots (3.b)$$

In 1961, Newmark and Hansen introduced a relationship to calculate the maximum blast pressure (P_{so}), in bars, for a high explosive charge detonates at the ground surface as:

$$Pso = 6784 \frac{W}{R3} + 93\left(\frac{W}{R^3}\right)^{1/2} \qquad \ldots\ldots\ldots\ldots\ldots (4)$$

In 1987, Mills introduces another expression of the peak overpressure in kpa, in which W is the equivalent charge weight in kilograms of TNT and Z is the scaled distance.

$$P_{so} = 1772/Z^3 - 114/Z^2 + 108/Z \quad \text{.....} \quad (5)$$

As the blast wave propagates through the atmosphere, the air behind the shock front is moving outward at lower velocity. The velocity of the air particles, and hence the wind pressure, depends on the peak overpressure of the blast wave. This later velocity of the air is associated with the dynamic pressure, $q(t)$. The maximum value, $q(s)$, say, is given by

$$q(s) = 5\, P_{so}2/2\, (P_{so}+7\, P_o) \quad \text{.....} \quad (6)$$

If the blast wave encounters an obstacle perpendicular to the direction of propagation, reflection increases the overpressure to a maximum reflected pressure Pr as:

$$P_r = 2\, P_{so}\, \{\frac{7\, Po + 4\, Pso}{7\, Po + Pso}\} \quad \text{.....} \quad (7)$$

A full discussion and extensive charts for predicting blast pressures and blast durations are given by Mays and Smith (1995) and TM5-1300 (1990). Some representative numerical values of peak reflected overpressure are given in Table 3.1.

Table 3.1. Peak reflected overpressures *Pr* (in MPa) with different W-R combinations

W / R	**100 kg TNT**	**500 kg TNT**	**1000 kg TNT**	**2000 kg TNT**
1m	165.8	354.5	464.5	602.9
2.5m	34.2	89.4	130.8	188.4
5m	6.65	24.8	39.5	60.19
10m	0.85	4.25	8.15	14.7
15m	0.27	1.25	2.53	5.01
20m	0.14	0.54	1.06	2.13
25m	0.09	0.29	0.55	1.08
30m	0.06	0.19	0.33	0.63

For design purposes, reflected overpressure can be idealized by an equivalent triangular pulse of maximum peak pressure *Pr* and time duration t_d, which yields the reflected impulse (i_r).

$$\text{Reflected Impulse } (i_r) = \frac{1}{2} P_r t_d \quad \text{……..8}$$

Duration t_d is related directly to the time taken for the overpressure to be dissipated. Overpressure arising from wave reflection dissipates as the perturbation propagates to the edges of the obstacle at a velocity related to the speed of sound (U_s) in the compressed and heated air behind the wave front. Denoting the maximum distance from an edge as *S* (for example, the lesser of the height or half the width of a conventional building), the additional pressure due to reflection is considered to reduce from $P_r - P_{so}$ to zero in time $3S/U_s$. Conservatively, U_s can be taken as the normal speed of sound, which is about 340 m/s, and the additional impulse to the structure evaluated on the assumption of a linear decay.

After the blast wave has passed the rear corner of a prismatic obstacle, the pressure similarly propagates on to the rear face; linear build-up over duration $5S/U_s$ has been suggested. For skeletal structures the effective duration of the net overpressure load is thus small, and the drag loading based on the dynamic pressure is then likely to be dominant. Conventional wind-loading pressure coefficients may be used, with the conservative assumption of instantaneous build-up when the wave passes the plane of the relevant face of the building, the loads on the front and rear faces being numerically cumulative for the overall load effect on the structure. Various formulations have been put forward for the rate of decay of the dynamic pressure

loading; a parabolic decay (i.e. corresponding to a linear decay of equivalent wind velocity) over a time equal to the total duration of positive overpressure is a practical approximation.

3.3 STRUCTURAL RESPONSE TO BLAST LOADING

Complexity in analyzing the dynamic response of blast-loaded structures involves the effect of high strain rates, the non-linear inelastic material behavior, the uncertainties of blast load calculations and the time-dependent deformations. Therefore, to simplify the analysis, a number of assumptions related to the response of structures and the loads has been proposed and widely accepted. To establish the principles of this analysis, the structure is idealized as a single degree of freedom (SDOF) system and the link between the positive duration of the blast load and the natural period of vibration of the structure is established. This leads to blast load idealization and simplifies the classification of the blast loading regimes.

3.3.1 ELASTIC SDOF SYSTEMS

The simplest discretization of transient problems is by means of the SDOF approach. The actual structure can be replaced by an equivalent system of one concentrated mass and one weightless spring representing the resistance of the structure against deformation. Such an idealized system is illustrated in Fig.5.1. The structural mass, M, is under the effect of an external force, $F(t)$, and the structural resistance, R_m, is expressed in terms of the vertical displacement, y, and the spring constant, K.

The blast load can also be idealized as a triangular pulse having a peak force F_m and positive phase duration t_d (see Figure 3.5). The forcing function is given as

$$F(t) = F_m\left(1 - \frac{t}{t_d}\right) \text{.....9}$$

The blast impulse is approximated as the area under the force-time curve, and is given by

$$I = \frac{1}{2} F_m t_d \qquad \text{.....10}$$

The equation of motion of the un-damped elastic SDOF system for a time ranging from 0 to the positive phase duration, t_d, is given by Biggs (1964) as

$$M\ddot{y} + Ky = F_m\left(1 - \frac{t}{t_d}\right) \text{.....11}$$

The general solution can be expressed as:

Displacement $y(t) = \frac{F_m}{K}(1 - \cos\omega t) + \frac{F_m}{Kt_d}\left(\frac{\sin\omega t}{\omega} - t\right)$ 12

Velocity $\dot{y}(t) = \frac{dy}{dt} = \frac{F_m}{K}\left[\omega \sin\omega t + \frac{1}{t_d}(\cos\omega t - 1)\right]$ 13

in which ω is the natural circular frequency of vibration of the structure and T is the natural period of vibration of the structure which is given by equation 14.

$$\omega = \frac{2\pi}{T} = \sqrt{\frac{K}{M}} \text{.....14}$$

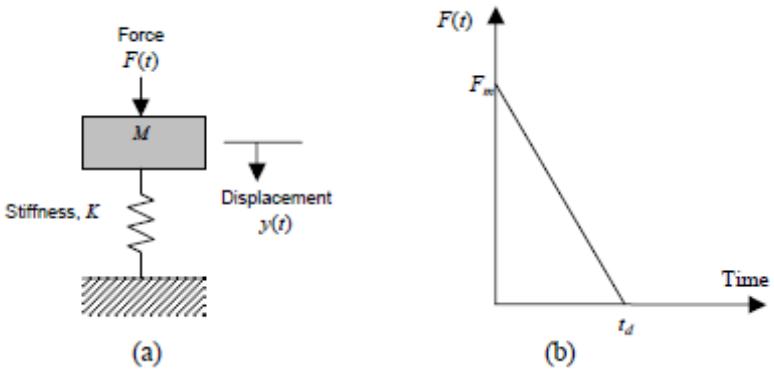

Figure 3.5 (a) SDOF system and (b) blast loading

The maximum response is defined by the maximum dynamic deflection y_m which occurs at time t_m. The maximum dynamic deflection y_m can be evaluated by setting dy/dt in Equation 12

equal to zero, i.e. when the structural velocity is zero. The dynamic load factor, DLF, is defined as the ratio of the maximum dynamic deflection y_m to the static deflection y_{st} which would have resulted from the static application of the peak load F_m, which is shown as follows:

$$DLF = \frac{Y_{\max}}{Y_{st}} = \frac{Y_{\max}}{F_m / K} = \psi(\omega t_d) = \psi\left(\frac{t_d}{T}\right) \ldots\ldots\ldots\ldots\ldots 15$$

The structural response to blast loading is significantly influenced by the ratio *td*/T or ωt_d (*td*/T = $\omega t_d / 2\pi$). Three loading regimes are categorized as follows:

- $\omega t_d < 0.4$: impulse loading resime.
- $\omega t_d < 0.4$: quasi-static resime.
- $0.4 < \omega t_d < 40$: dynamic loading resime.

3.3.2 ELASTO-PLASTIC SDOF SYSTEMS

Structural elements are expected to undergo large inelastic deformation under blast load or high velocity impact. Exact analysis of dynamic response is then only possible by step-by-step numerical solution requiring nonlinear dynamic finite- element software. However, the degree of uncertainty in both the determination of the loading and the interpretation of acceptability of the resulting deformation is such that solution of a postulated equivalent ideal elasto-plastic SDOF system (Biggs, 1964) [6] is commonly used. Interpretation is based on the required ductility factor $\mu = y_m/y_e$. For example, uniform simply supported beam has first mode shape $\varphi(x) = \sin \pi x/L$ and the equivalent mass $M = (1/2)mL$, where L is the span of the beam and m is mass per unit length.

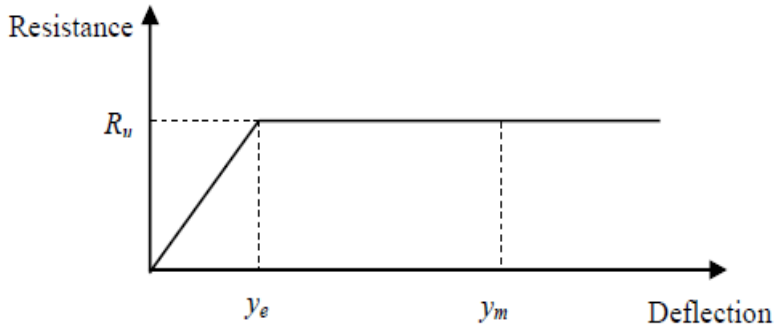

Figure 3.6 Simplified resistance function of an elasto-plastic SDOF system

The equivalent force corresponding to a uniformly distributed load of intensity p is $F = (2/\pi)pL$. The response of the ideal bilinear elasto-plastic system can be evaluated in closed form for the triangular load pulse comprising rapid rise and linear decay, with maximum value Fm and duration td. The result for the maximum displacement is generally presented in chart form TM 5-1300 [23], as a family of curves for selected values of Ru/Fm showing the required ductility μ as a function of td/T, in which Ru is the structural resistance of the beam and T is the natural period (Figure 3.7).

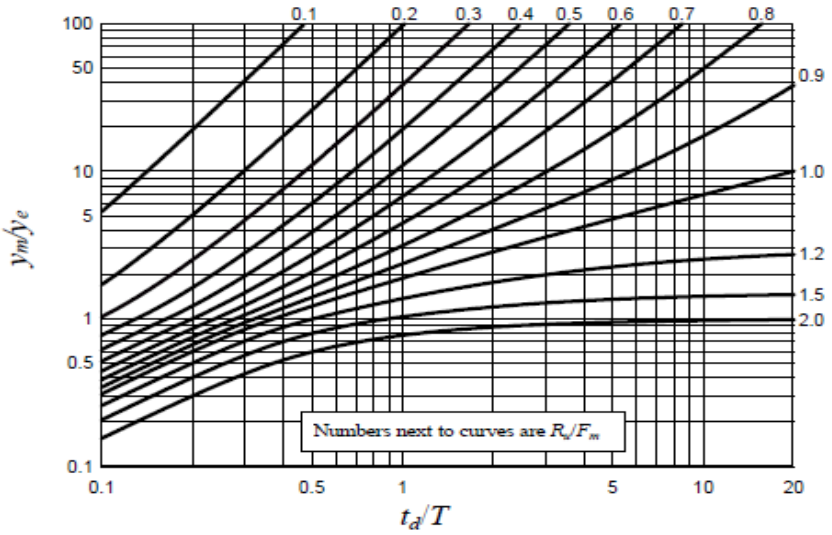

Figure 3.7 Maximum response of elasto-plastic SDF system to a triangular load.

3.4 MATERIAL BEHAVIORS AT HIGH STRAIN RATE

Blast loads typically produce very high strain rates in the range of 10^2 - 10^4 s^{-1}. This high loading rate would alter the dynamic mechanical properties of target structures and, accordingly, the expected damage mechanisms for various structural elements. For reinforced concrete structures subjected to blast effects the strength of concrete and steel reinforcing bars can increase significantly due to strain rate effects. Figure 3.8 shows the approximate ranges of the expected strain rates for different loading conditions. It can be seen that ordinary static strain rate is located in the range: 10^{-6}-10^{-5} s^{-1}, while blast pressures normally yield loads associated with strain rates in the range: 10^2-10^4 s^{-1}.

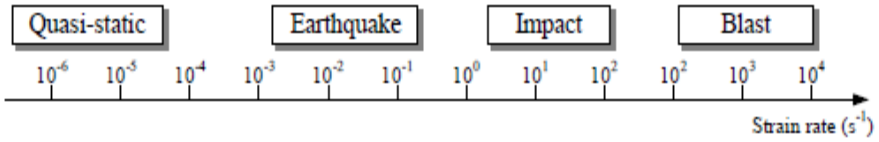

Figure 3.8 Strain rates associated with different types of loading.

3.4.1 DYNAMIC PROPERTIES OF CONCRETE UNDER HIGH-STRAIN RATES

The mechanical properties of concrete under dynamic loading conditions can be quite different from that under static loading. While the dynamic stiffness does not vary a great deal from the static stiffness, the stresses that are sustained for a certain period of time under dynamic conditions may gain values that are remarkably higher than the static compressive strength (Figure 3.9). Strength magnification factors as high as 4 in compression and up to 6 in tension for strain rates in the range: 10^2–10^3 /sec have been reported (Grote et al., 2001) [9].

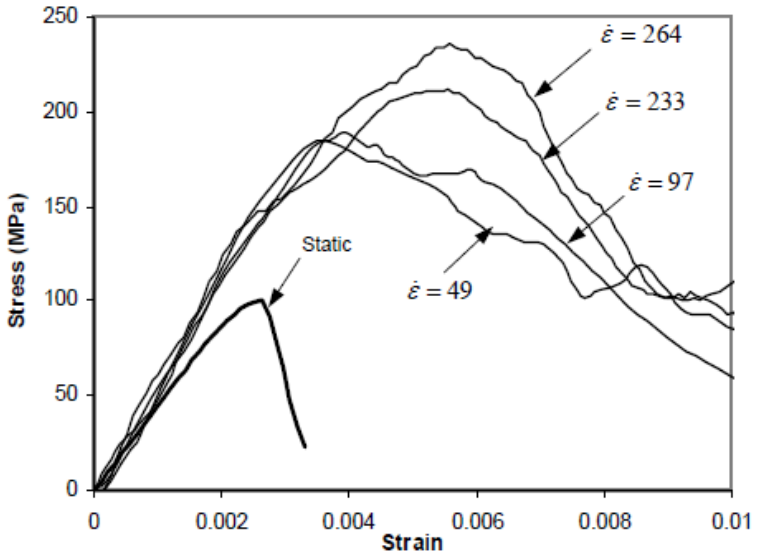

Figure 3.9 Stress-strain curves of concrete at different strain rates. [9]

For the increase in peak compressive stress (*f'c*), a dynamic increase factor (DIF) is introduced in the CEB-FIP (1990) model (Figure 3.10) for strain-rate enhancement of concrete as follows:

$$DIF = \left\{\frac{\dot{\varepsilon}}{\dot{\varepsilon}_s}\right\}^{1.026\alpha} \quad \text{for} \quad \dot{\varepsilon} \le 30s^{-1} \qquad \ldots\ldots\ldots 16$$

$$DIF = \gamma\left\{\frac{\dot{\varepsilon}}{\dot{\varepsilon}_S}\right\}^{1/3} \quad \text{for} \quad \dot{\varepsilon} \le 30s^{-1} \qquad \ldots\ldots\ldots 17$$

where:

$\dot{\varepsilon}$ = strain rate ,

$\dot{\varepsilon}_s = 30\times10^{-6}s^{-1}$ (quasi-static strain rate)

$\log y = 6.156\ \alpha - 2$

$\alpha = 1/(5 + 9\ f'c/fco)$

fco = 10 MPa = 1450 psi

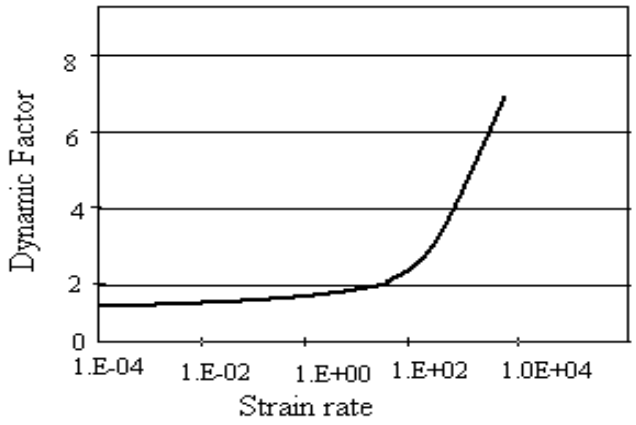

Figure 3.10 Dynamic Increase Factor (DIF) for peak stress of concrete.

3.4.2 DYNAMIC PROPERTIES OF REINFORCING STEEL UNDER HIGH-STRAIN RATES

Due to the isotropic properties of metallic materials, their elastic and inelastic response to dynamic loading can easily be monitored and assessed. Norris et al. (1959)[24] tested steel with two different static yield strength of 330 Mpa and 278 MPa under tension at strain rates ranging from 10^{-5} to $0.1s^{-1}$ [24]. Strength increase of 9 - 21% and 10 - 23 % were observed for the two steel types, respectively. Dowling and Harding (1967) conducted tensile experiments using the tensile version of Split Hopkinton's Pressure Bar (SHPB) on mild steel using strain rates varying between 10^{-3} $s^{-1}$and 2000 s^{-1} [24]. It was concluded from this test series that materials of body-centered cubic (BCC) structure (such as mild steel) showed the greatest strain rate sensitivity. It has been found that the lower yield strength of mild steel can almost be doubled; the ultimate tensile strength can be increased by about 50%; and the upper yield strength can be considerably higher. In contrast, the ultimate tensile strain decreases with increasing strain rate. Malvar (1998) also studied strength enhancement of steel reinforcing bars under the effect of high strain rates [24]. This was described in terms of the dynamic increase factor (DIF), which can be evaluated

for different steel grades and for yield stresses, *fy*, ranging from 290 to 710 MPa as represented by equation 18.

$$DIF = \left(\frac{\dot{\varepsilon}}{10^{-4}} \right)^{\alpha} \quad \text{.....18}$$

Where for calculating yield stress $\alpha = \alpha_{fy}$

$\alpha_{fy} = 0.074 - 0.04(f_y/414)$…….19

For ultimate stress calculation $\alpha = \alpha_{fy}$

$\alpha_{fy} = 0.019 - 0.009(f_y/414)$…….20

Chapter – 4

DYNAMIC LOADING ON STRUCTURES

Chapter 4

DYNAMIC LOADING ON STRUCTURES

4.1 COMPUTATION OF DYNAMIC LOADING ON CLOSED RECTANGULAR STRUCTURES

Let it be assumed that it is required to determine the average net horizontal pressure P_{net} that acts on the rectangular aboveground building in Fig 4-1. The dimensions of the building are shown in the same figure. The structure is assumed to be subjected to a peak overpressure P_{so}=5.45psi, which is produced by a weapon yield of 1.2 kilotons.

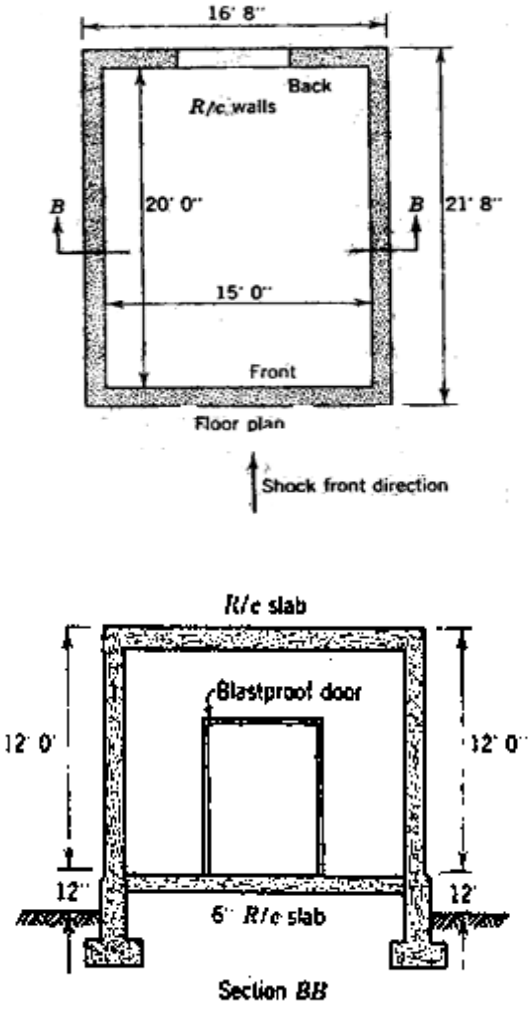

Figure 4-1 Closed rectangular structure.

The shock front velocity U_o is,

$$U_o = 1117\left[1+\frac{6P_{so}}{7P_o}\right] \ldots\ldots\ldots\ldots\ldots\ldots\ldots 21$$

$$U_o = 1117\left[1+\frac{6(5.45)}{7(14.7)}\right]^{\frac{1}{2}} = 1283\, fps$$

From Fig 4.2, the positive phase duration (t_{o1}) of the overpressure P_s for 1 kiloton weapon yield is 0.314 sec.

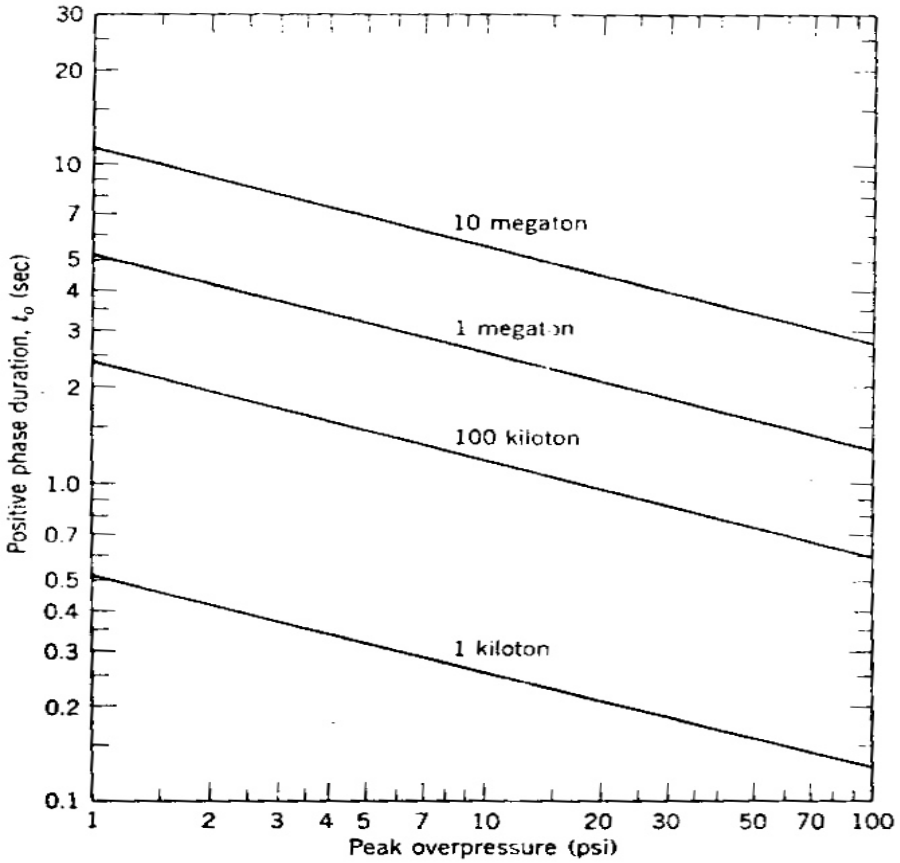

Figure 4-2 Positive phase duration of overpressure for surface burst.

For 1.2 kilotons, the positive phase duration (t_{o2}) can be computed from Eq. 22. That is,

$$t_{o2} = t_{o1}(Z)^{1/3} \quad \ldots\ldots\ldots\ldots\ldots\ldots 22$$

$$t_{o2} = (0.314)(1.2)^{1/3} = 0.33 \text{ sec}$$

The peak dynamic pressure (P_{do}) can be determined from Fig. 4-3. With P_{so}=5.45 psi, the range d_1 for a 1-kiloton weapon is 1400.00 ft. In the same figure, the same range, the peak dynamic pressure P_{do} is 0.65 psi.

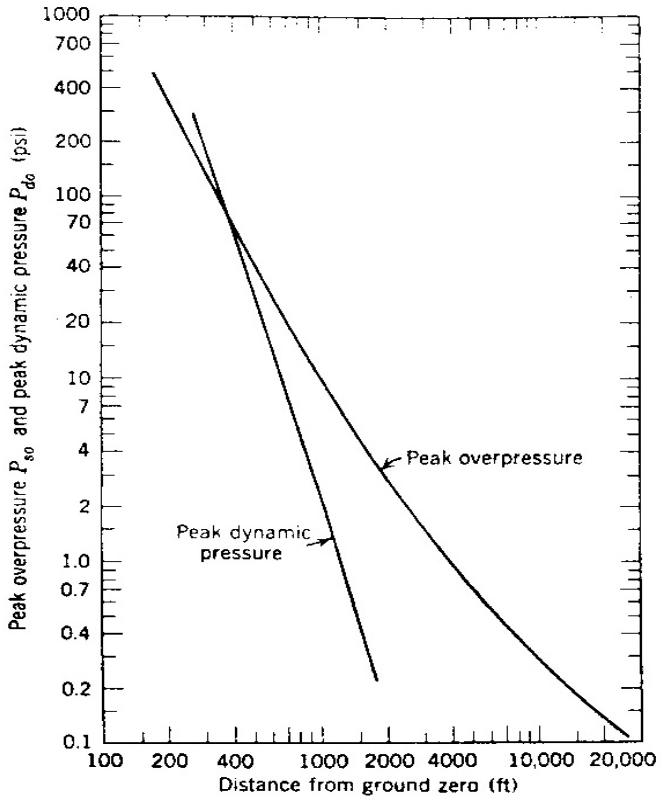

Figure 4-3 Peak overpressure and peak dynamic pressure for surface burst.

For 1.2 kilotons, the range (d) can be found from Eq. 23. That is,

$$d = d_1(Z)^{1/3} \quad \ldots\ldots\ldots\ldots 23$$

$$d = (1400)(1.2)^{1/3} = 1485 \text{ ft}$$

The positive phase duration (t_{od1}) of the dynamic pressure (P_d) for 1-kiloton weapon yield can be found from Fig.4-4. Thus, with d_1=1400 ft, Fig. 4-4 yields t_{od1}=0.39 sec.

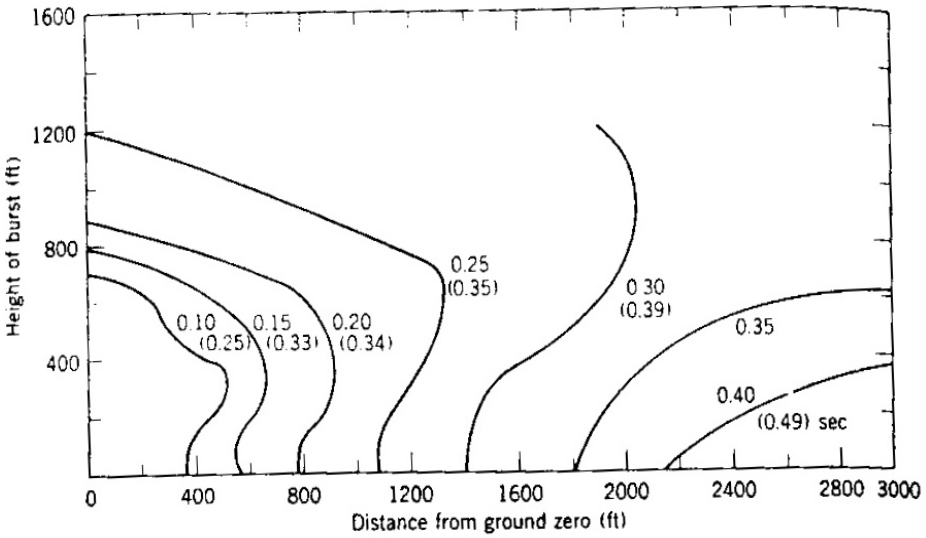

Figure 4-4. Positive phase duration of overpressure and dynamic pressure (in parenthesis)

From Eq. 24, the positive phase duration (t_{od}) for 1.2 kilotons is,

$$t_{od} = t_{od1}(Z)^{1/3} \text{ ……..24}$$

$$t_{od} = (0.39)(1.2)^{1/3} = 0.41 \sec$$

The peak reflected overpressure (P_r) is given by Eq. 25. Thus

$$P_r = 2P_{so}\left(\frac{7P_o + 4P_{so}}{7P_o + P_{so}}\right) \text{ ……25}$$

$$P_r = (2)(5.45)\left[\frac{(7)(14.7)+(4)(5.45)}{(7)(14.7)+(5.45)}\right] = 12.56\,psi$$

From Eq. 26, with $U_r=U_o=1283$ fps, the clearing time (t_c) is,

$$t_c = \frac{3S}{U_r} \text{.....26;} \quad t_c = \frac{(3)(8.33)}{1283} = 0.0195 \text{sec}$$

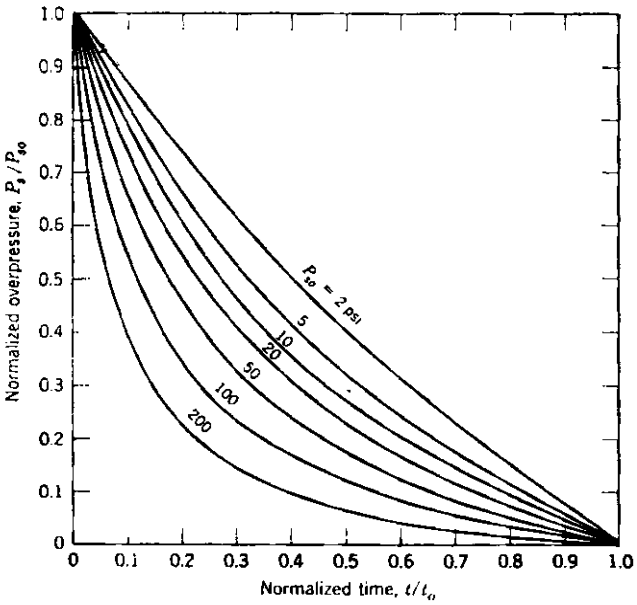

Figure 4-5. Rate of decay of overpressure for various values of P_{so}

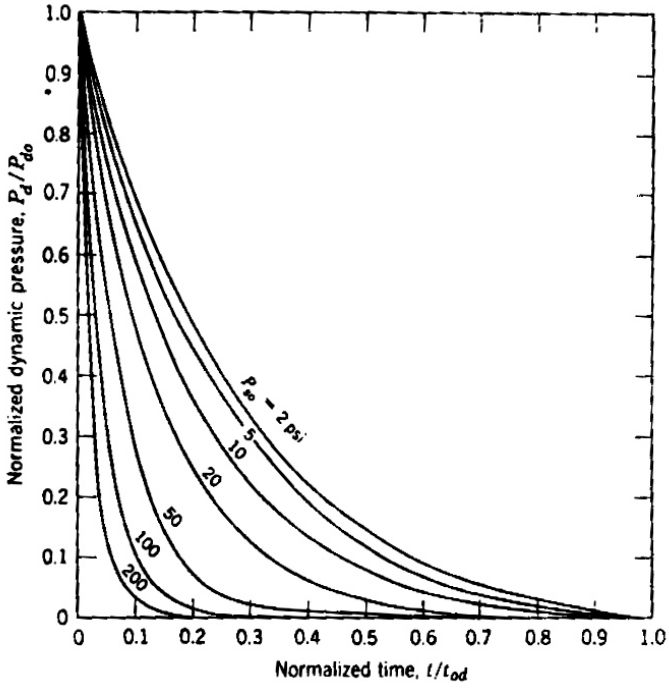

Figure 4-6. Rate of decay of dynamic pressure for various values of P_{so}

4.1.1 AVERAGE PRESSURE ON FRONT FACE

The variation of the average pressure (P_{front}) of the front face can be easily determined. For simplicity it is assumed that t_{o2}= t_{od} = 0.33 sec. This is a fair approximation, because the difference between t_{o2} and t_{od} is not large and the dynamic pressure (P_d) is rather small compared to the overpressure (P_s). At t= 0, the pressure (P_{front}) in Fig.4-7, is equal to P_r . At t = t_c = 0.0195 sec, the values of P_s and P_d can be determined from Figs.4-5 and 4-6, respectively. If preferred, Eqs. 27 and 28 can be used because P_{so} and P_{do} are less than 10 psi. Thus at t = t_c = 0.0195 sec, P_s and P_d are 4.75 and 0.51 psi respectively, Therefore, at t = t_c,

$$P_s = P_{so}\left(1-\frac{t}{t_o}\right)e^{-t/to} \qquad (\text{for } P_{so} < 10)\ldots\ldots\ldots\ldots\ldots\ldots 27$$

$$P_d = P_{do}\left(1-\frac{t}{t_{od}}\right)e^{-2t/t_{od}} \quad (\text{for } P_{do} < 10)\ldots\ldots\ldots\ldots\ldots\ldots 28$$

$$P_{fornt} = P_s + C_d\left(P_d\right)\ldots\ldots\ldots\ldots\ldots\ldots\ldots 29$$

$$P_{front} = 4.75 + (0.85)(0.51) = 5.18\,psi$$

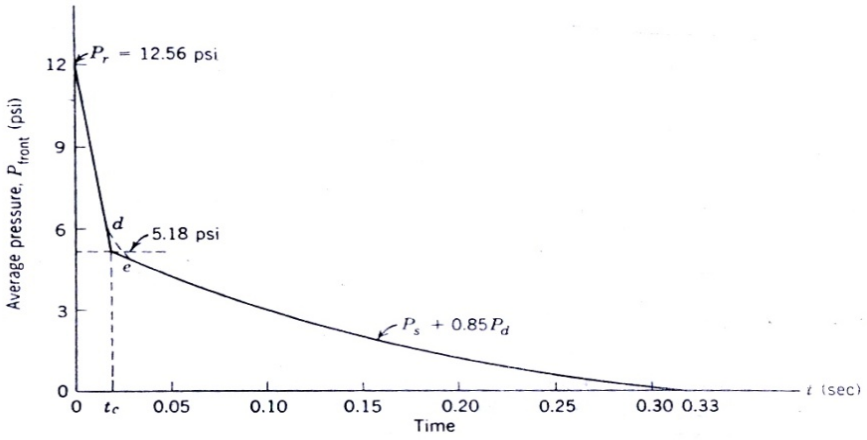

Figure4-7, Average front face pressure verses time.

The value of P_{front} for the time interval between $t = t_c$ and $t = 0.33$ sec are equal to $P_s + 0.85\ P_d$. In Fig.4-7, the variation of P_{front} between t= 0 and $t = t_c$ is assumed to be linear. The incompatible discontinuity at $t = t_c$, if preferred, can be smoothed out by the fairing curves *de* shown by a dashed line

4.1.2 AVERAGE PRESSURE ON BACK FACE

The time t_d at which the shock front arrives at the back face of the building is,

$$t_d = \frac{L}{U_o} = \frac{21.67}{1283} = 0.017 \text{ sec} \quad \ldots\ldots\ldots\ldots\ldots 30$$

The time t_b that is required for the average pressure P_{back} to build up to its maximum value $(P_{back})_{max}$ is,

$$t_b = \frac{4S}{U_o} = \frac{(4)(8.33)}{1283} = 0.026 \text{ sec} \quad \ldots\ldots\ldots\ldots\ldots 31$$

With $t = t_b = 0.026$ sec and $t_o = t_{o2} = 0.33$ sec, the value P_{sb} of the overpressure P_s can be determined from either Eq. 27 or Fig.4-5. The result is,

From equation 27,

$$P_{sb} = P_{so}\left(1 - \frac{t_b}{t_{ob}}\right)e^{-t_o/t_{ob}}$$

$$P_{sb} = 5.45\left(1 - \frac{0.026}{0.33}\right)e^{-0.026/0.33} = 4.47\,psi$$

$$\left(P_{back}\right)_{\max} = \frac{P_{sb}}{2} + \left[1 + (1-\beta)e^{-\beta}\right] \text{.....32}$$

$$\beta = \frac{0.5P_{so}}{P_o} = \frac{(0.5)(5.45)}{14.7} = 0.186$$

$$\left(P_{back}\right)_{\max} = \frac{4.47}{2}\left[1 + (1-0.186)e^{-0.186}\right] = 3.75\,psi$$

The variation of P_{back} for the time interval $t_d \le t \le (t_d + t_b)$ is assumed to be linear. The variation in the time interval $(t_d + t_b) \le t \le (t_{o2} + t_d)$ can be computed from Eq. 33. For example, at t= 0.070 sec, then

$$\frac{P_{back}}{P_s} = \frac{\left(P_{back}\right)_{\max}}{P_{sb}} + \left[1 - \frac{\left(P_{back}\right)_{\max}}{P_{sb}}\right]\left[\frac{t - (t_d + t_b)}{t_o - t_b}\right]^2 \text{.....33}$$

$$\frac{P_{back}}{P_s} = \frac{3.75}{4.47} + \left[1 - \frac{3.75}{4.47}\right]\left[\frac{0.070 - (0.017 + 0.026)}{0.330 - 0.026}\right]^2 = 0.839$$

or $P_{back} = 0.839\ P_s$

From Fig.4-5, with $t / t_o = t - t_d / t_{o2} = 0.070 - 0.017 / 0.330 = 0.161$, the value of the overpressure (P_s) is,

$$P_s = 0.716P_{so} = (0.716)(5.45) = 3.90\,psi$$

Thus, at t = 0.070 sec,

$$P_{back} = 0.839P_s = (0.839)(3.90) = 3.27\,psi$$

In a similar manner, the values of P_{back} for other time t can be obtained. The complete results are shown plotted in Fig.4-8.

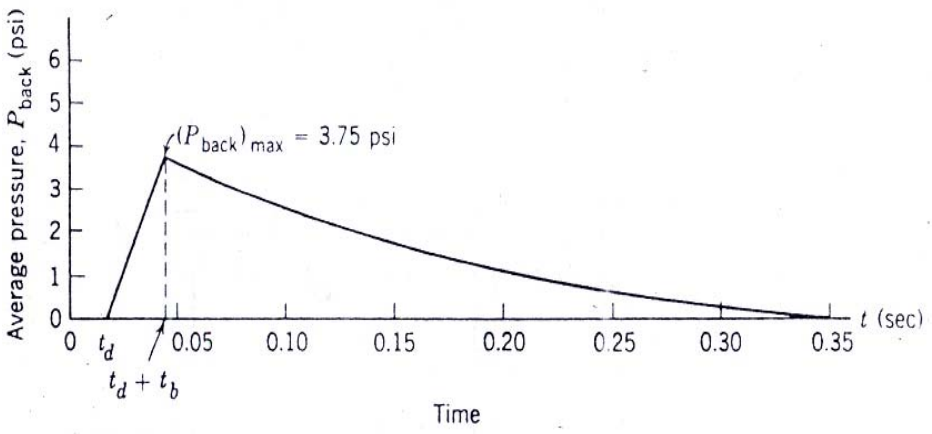

Figure 4-8, Average back face pressure versus time.

4.1.3 AVERAGE NET HORIZONTAL PRESSURE

The average net horizontal pressure P_{net} is given by,

$$P_{net} = P_{front} - P_{back} \text{ ……..34}$$

The value of pressure in Fig.4-8, are subtracted from the corresponding values in Fig.4-7, the variation of the net horizontal pressure in Fig.4-9, is obtained.

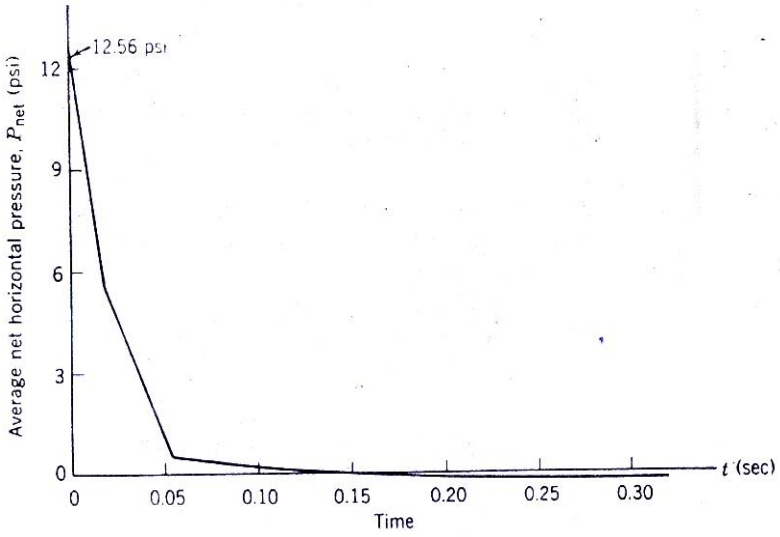

Figure 4-9, Average net horizontal pressure versus time.

4.1.4 AVERAGE PRESSURE ON ROOF AND SIDES

For the rectangular building in Fig.4.1

$$\frac{L}{U_o} = \frac{21.67}{1283} = 0.017 \text{ sec}$$

And

$$\frac{L}{2U_o} = \frac{21.67}{(2)(1283)} = 0.0085 \text{ sec}$$

The average pressure on the side and roof is,

$$P_m = P_s(t = 0.0085) + C_d P_d(t = 0.0085) \ldots\ldots\ldots\ldots\ldots 35$$

$$P_m = 5.12 + (-0.4)(0.56) = 4.90 psi$$

Where the Ps and Pd are computed by using Fig.4-5 and 4-6 respectively, the complete variation of the average pressure on the sides and the roof of the rectangular building in Fig.4.1 verses time is shown in Fig.4-10.

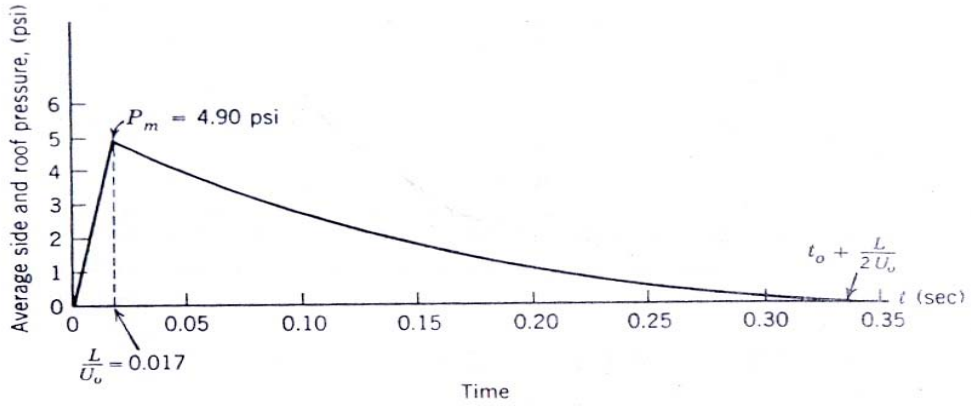

Figure 4-10 Average side and roof pressure versus time.

4.2 DYNAMIC LOADING ON RECTANGULAR STRUCTURES WITH OPENINGS

The structures included in this category are the ones whose front and back faces have at least 30% of openings or windows area and have no interior partitions to block or influence the passage of the blast wave. The average pressure on the outside of the front face can be computed in the same manner as for closed rectangular structures, except that *S* in Eq. 26 is replaced by *S'*. The quantity *S'* is the weighted average distance that the rarefaction wave must travel in order to cover the wall once, provided that the blast wave has immediate access to the interior of the structure. This is not an unreasonable assumption, because the windows and doors usually break before the clearing of the reflected overpressure is completed.

The distance *S'* can be computed from the expression

$$S' = \sum \frac{\delta_n h_n A_n}{A_f} \leq S \quad \text{.....36}$$

To understand the meaning of the symbols in Eq.36, consider the front face in Fig. 4-11 which has two opening.

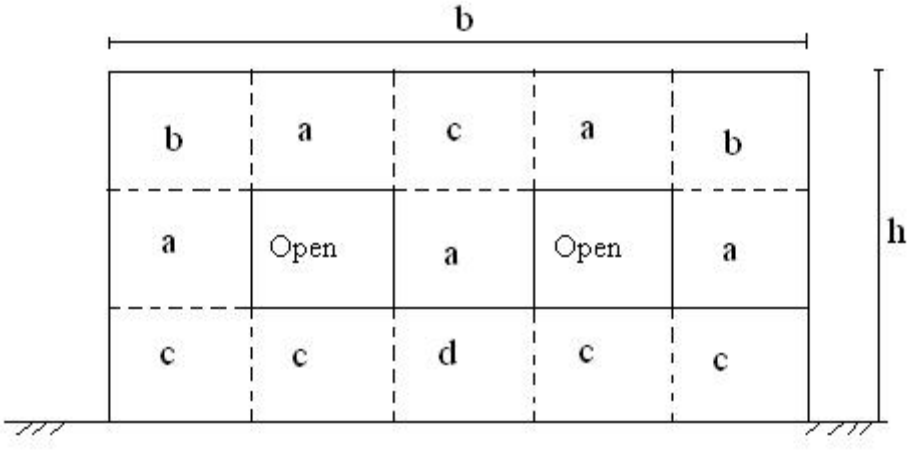

Figure 4-11 Subdivision of a typical wall with openings.

The face is divided into rectangular areas as shown. The areas cleared from two opposite sides are marked α, while b and c are the areas cleared from two adjacent sides and one side, respectively. The remaining areas are marked d.

On this basis In Eq. 36,

A_f is the area of the front face less the area of the openings.

A_n is the area of each of portions of the subdivide front face, except openings.

h_n for areas α, is the average distance between the sides from which clearing occurs.

for areas b and d, is the average height or width, whichever is smaller.

for areas c, is the average distance between the side from which clearing occurs and the side opposites.

δ_n is the clearing factor that has the value 0.5 for areas α, and it is equal to unity for areas b, c and d.

The average pressure on the inside of the front face is zero at t = 0 and it takes a time $2L/U_o$ to reach the value P_s of the blast wave overpressure. The dynamic pressures P_d are assumed to be negligible on the interior of the structure. The variation with time of the average pressure of the inside and the outside of the front face are shown in Fig. 4-12.

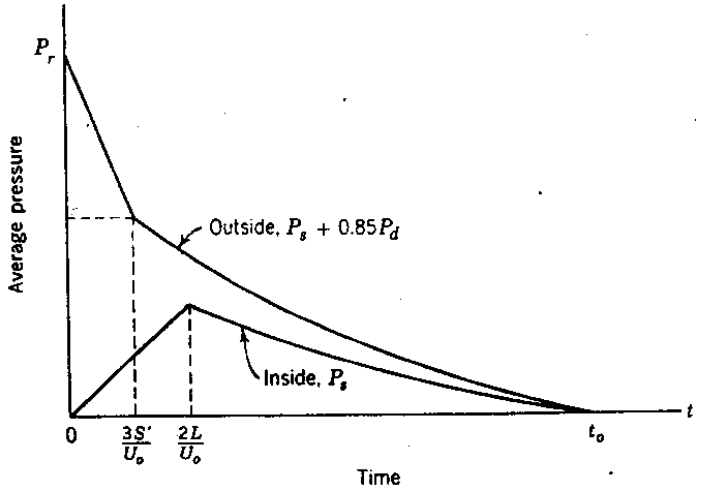

Figure 4-12 Time variation of front face average pressure

For the sides and top, the outside average pressure obtained as for a closed structure. The inside pressure, as for the front face, require a time $2L/U_o$ to attain the overpressure of the blast wave. Here again the dynamic pressure in the interior are neglected. The variations of the pressure with time are shown in Fig. 4-13.

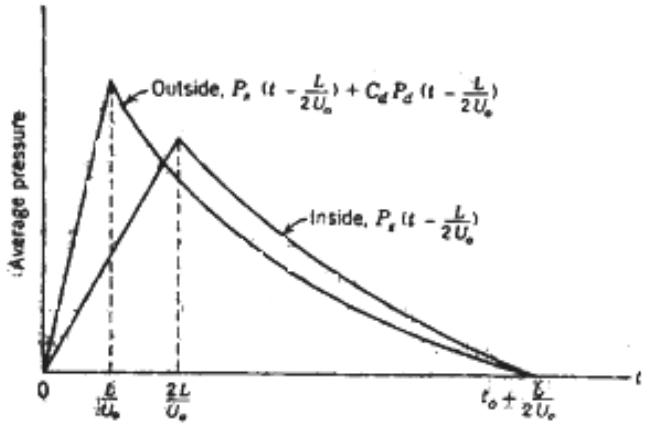

Figure 4-13 Time variations of side and top average pressures.

For the back face, the outside pressure is the same as for the closed structure, but with *S* replaced by *S'* where *S'* is given by Eq. 36. The inside pressure is reflected from the inside of the back face and it takes a time equal to L/U_o to reach the same value as the blast overpressure. For times in excess of L/U_o, the inside pressure decays as P_s (t-L/U_o). The dynamic pressure is assumed to be negligible. The variations of the these pressure with time are shown in Fig.4-14

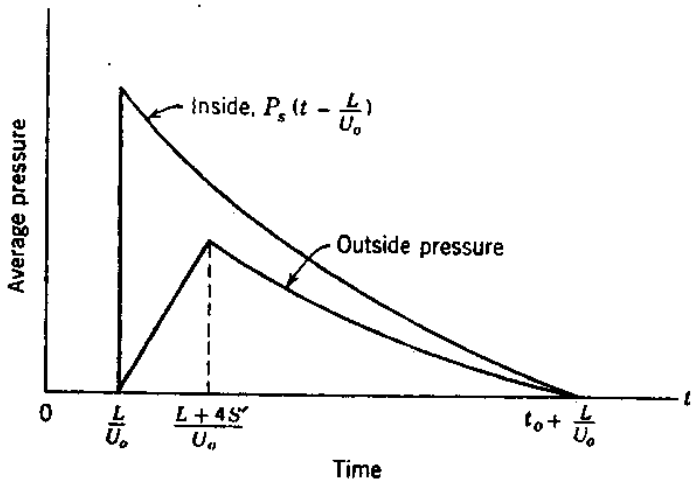

Figure 4-14 Time variation of back face average pressure

The net horizontal loading is equal to the net front face loading, that is outside minus inside, and minus the net back face loading.

4.3 DYNAMIC LOADING ON OPEN-FRAME STRUCTURES

An open-frame structure is one whose structural elements are exposed to a blast wave. For example, steel-frame office buildings whose wall areas are mostly glass, truss bridges and so on, are classified as open-frame structures. Before the frangible material breaks, it will transmit some loading to the frame. This loading is assumed to be negligible if the frangible material is glass, provides that the blast loading is sufficiently large to fracture the glass. If the frangible material is asbestos, corrugated steel or aluminum paneling, an approximate value of the load transmitted to the frame is an impulse of 0.04 lb-sec/ in^2. When the frangible material breaks, the frame of the structure are directly subjected to the effects of the blast wave.

A simplification of the problem would be to treat the overpressure loading as an impulse. The value of this impulse is first computed for an average member in the same way as foe a closed structure, and the result is multiplied by the number of members. This impulse is assumed to be delivered as soon as the shock front strikes the structure. If preferred, it can be separated into two impulses – one for the front face and one for the back face as shown in Fig. 4-15. The symbols A_{fw} and A_{bw} represent the areas of the front and back walls respectively, which transmit loads before failure, and I_{fm} and I_{bm} are the overpressure loading impulses on the front and back members. The major portion of the loading on an open-frame structure is the drag loading. The drag coefficient C_d for an individual member in the open whose section is an *I*-beam, angle or rectangle, is about 1.5.

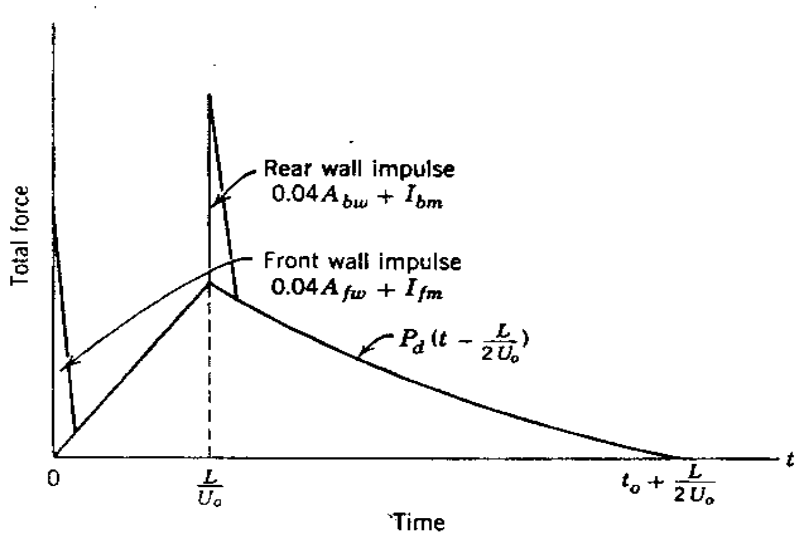

Figure 4-15 Net horizontal loading of an open frame structure.

When the whole frame is considered, the average drag coefficient is reduced to 1.0, because the various members shield one another to a certain extent from the effects of the full blast loading. Thus, on an individual member, the force F, that is, pressure multiplied by area, is given by the expression.

$$F_{member} = C_d P_d A_i \quad \text{.....37}$$

Where Ai = the area of the member that is projected perpendicular to the direction of

propagations of the blast wave, and

C_d =1.5

For the loading on a frame, the force *F* is

$$F_{frame} = C_d P_d \sum A_i = C_d P_d A \quad \text{.....38}$$

Where C_d = 1.0 and

$\sum A_i = A$ is the sum of the projected area of all the members.

The drag force attains its full value at the time L/U_o, that is, when the blast wave reaches the end of the structure.

Chapter – 5

FINITE ELEMENT MODEL

Chapter 5

FINITE ELEMENT MODEL

5.1 INTRODUCTION

This chapter covers the details of element types, material models to be considered to create finite element model for Reinforced concrete by using ANSYS finite element software. A brief introduction about the type of nonlinearities in structural components, stress-strain curve for concrete and steel, and details of different models adopted for assessing the ultimate load carrying capacity have been discussed.

5.2 STRUCTURAL NONLINEARITY

Nonlinear analysis of reinforced concrete structures has become increasingly important in recent years. It is only by carrying out a complete progressive failure analysis of the structure up to collapse that it is possible to assess all safety aspects of a structure and to find its deformational characteristics. Care must be taken to select the load steps during the nonlinear analysis.

With the present state of development of computer programs based on the finite element, modeling issues of reinforced concrete material is often one of the major factors in limiting the capability of structural analysis. This is because reinforced concrete has a very complex behavior involving phenomena such as inelasticity, cracking, time dependency and interactive effects between concrete and reinforcement. The development of material models for uncracked and cracked concrete for all stages of loading is a particularly challenging field in nonlinear analysis of reinforced concrete structures.

The major sources, which are responsible for the nonlinear behavior of reinforced concrete, are (Chen and Saleeb [25])

1. Cracking of concrete

2. Plasticity of the reinforcement and of the compression concrete

3. Time dependent effects such as creep, shrinkage, temperature, and load history.

5.3 NONLINEARITIES IN REINFORCED CEMENT CONCRETE

The behavior of R.C.C cannot be modeled properly by linear elastic behavior. Recognizing this, the design of R.C.C structures has gradually shifted over the years from the elastic working stress design to the more rational ultimate strength design. The nonlinearities in R.C.C members can be geometric as well as material. Both of these become very important at higher level of deformations.

5.3.1 GEOMETRIC NONLINEARITY

Linear structural analysis is based on the assumption of small deformations and the material behavior is considered linear elastic. The analysis is performed on the initial undeformed shape of the structure. As the applied loads increase, this assumption is no longer accurate, because the deformation may cause significant changes in the structural shape. Geometric nonlinearity is the change in the elastic deformation characteristics of the structure caused by the change in the structural shape due to large deformations.

For example in one dimensional flexural members modeled by the ‘Euler-Bernouli Beam’, the geometric nonlinearity can be reasonably represented by approximating the strains up

to second order terms. This causes a change in the stiffness matrix (with additional nonlinear terms, i.e., function of displacements) and the resulting analysis needs to be performed by iterative methods, like direct iteration or the Newton-raphson method.

In R.C.C structures, among the varies types of geometric nonlinearity, the structural instability or moment magnification caused by large compressive forces, stiffening of structures caused by large tensile forces, change in structural parameters due to applied loads are significant.

5.3.2 MATERIAL NONLINEARITY

Concrete and steel are two constituents of R.C.C. Among them, concrete is much stronger in compression than in tension (tensile strength is of the order of one tenth of the compressive strength). While the tensile stress –strain relationship of concrete is almost linear; the stress-strain relationship in compression is nonlinear from the beginning. Since the concrete and steel are both strongly nonlinear materials, the material nonlinearity of R.C.C is a complex combination of both.

5.4 STRESS-STRAIN CURVES OF CONCRETE AND STEEL

5.4.1 STRESS-STRAIN CURVES OF CONCRETE

Typical stress-strain curves of concrete of various grades, obtained from standard uniaxial compression tests are shown in Figure 5.1(Pillai and Menon [17]). The curves are somewhat linear in the very initial phase of loading; the nonlinearity begins to gain significance when the stress level exceeds about one-third of the maximum. The maximum stress is reached

at a strain approximately equal to 0.002; beyond this point, an increase in strain is accompanied by a decrease in stress. For the usual range of concrete strengths, the strain at failure is in the range of 0.003 to 0.005.

When the stress level reaches 90-95 percent of the maximum, internal cracks are initiated in the mortar throughout the concrete mass, roughly parallel to the direction of the applied loading. The concrete tends to expand laterally, and longitudinal cracks become visible when the lateral strain (due to poisson's effect) exceeds the limiting tensile strain of concrete 0.0001.

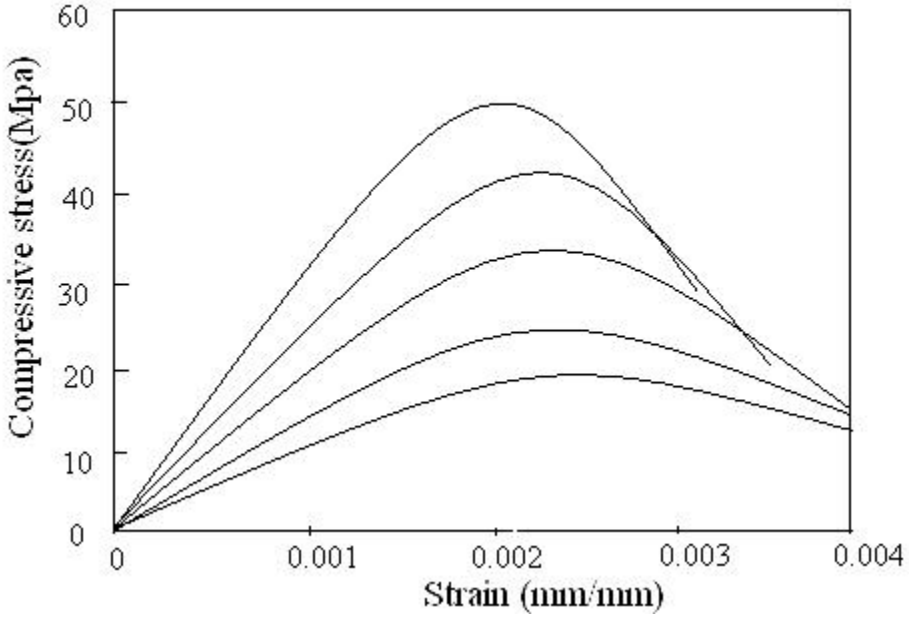

Figure 5.1 Stress-strain curves of concrete in compression

From the above curves one can conclude that higher the concrete grade, the steeper is the initial portion of the stress-strain curve, the sharper the peak of the curve, and the lesser the failure strain.

5.4.1.1 MODULUS OF ELASTICITY & POISSON'S RATIO

The Young's modulus of elasticity is defined as within the linear elastic range, the ratio of axial stress to the axial strain under uniaxial loading. The code IS-456 gives the following empirical expression for the static modulus in terms of the characteristic cube strength f_{ck} (in N/mm^2).

$$E_C = 5000\sqrt{f_{ck}}$$

The Poisson's Ratio is defined as the ratio of the lateral strain to the longitudinal strain, under uniform axial stress. Generally the poisson's ratio value for concrete lies between 0.1 to 0.3.

5.4.2 STRESS-STRAIN CURVE OF STEEL

Steel, when subjected to high stress levels, shows plasticity behavior, i.e. when all the forces acting on the body are removed, the body does not return its original shape, but has some permanent plastic deformation associated with it. Typical uniaxial stress-strain curves are as shown in Figure 5.2 for various grades of steel.

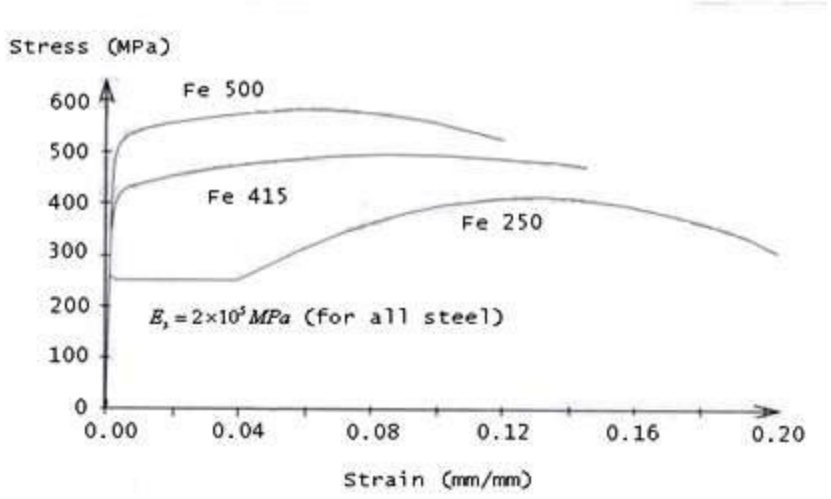

Figure 5.2 Uniaxial Stress-Strain curves of different steels

Modulus of elasticity of steel (E_S) in the initial linear elastic portion is $2 \times 10^5 N / mm^2$ (IS-456). An abrupt change in the modulus of the structure is observed for the material beyond the yield point. Moreover, upon unloading the material at any point beyond the yield point, a permanent deformation is introduced. This kind of behavior can be idealized by a bilinear stress-strain relationship with two slopes, the second slope being called the tangential modulus (E_T). After reaching the yield point, the slope could be less than, equal to, or greater than zero.

5.5 MODELING USING ANSYS

ANSYS is general-purpose finite element software for numerically solving a wide variety of structural engineering problems. The ANSYS element library consists of more than 100 different types of elements. For the numerical simulation of any RC structure, three dimensional solid element SOLID65 has been used for modeling the nonlinear behavior of concrete, three dimensional spar element LINK8 has been used for modeling the reinforcement.

5.5.1 SOLID65

Solid65 is used for the 3-Dimensional modeling of concrete with or without reinforcing bars. The solid is capable of cracking in tension and crushing in compression. The element is defined by eight nodes having three degrees of freedom at each node: translations in the nodal x, y, and z directions. The element is capable of accommodating three different rebar specifications. The most important aspect of this element is the treatment of nonlinear material properties. The concrete is capable of cracking (in three orthogonal directions), crushing, plastic deformation, and creep. The rebar's are capable of tension and compression, but not shear. The element is shown in Figure 5.3.

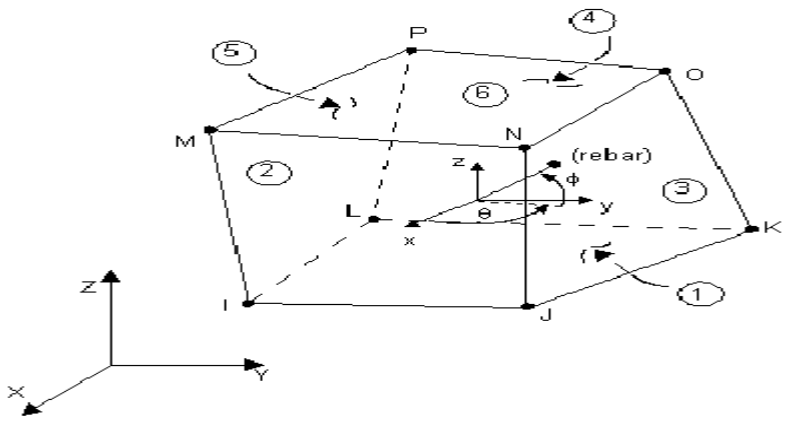

Figure 5.3 (a) SOLID65 Element

Typical shear transfer coefficients range from 0.0 to 1.0, with 0.0 representing a smooth crack (complete loss of shear transfer) and 1.0 representing a rough crack (no loss of shear transfer). In ANSYS, outputs, i.e., stresses and strains, are calculated at integration points of the concrete solid elements. A cracking sign represented by a circle appears when a principal tensile stress exceeds the ultimate tensile strength of the concrete. The cracking sign appears perpendicular to the direction of the principal stress.

Assumptions:

All elements must have eight nodes. Whenever the rebar capability of the element is used, rebars are assumed to be "smeared" throughout the element. The element is nonlinear and requires an iterative solution. When both cracking and crushing are used together, care must be taken to apply the load slowly to prevent possible fictitious crushing of the concrete before proper load transfer can occur through a closed crack.

5.5.2 LINK8

Link8 is a 3-dimensional spar (or truss) element. This element is used to model the steel in reinforced concrete. The three-dimensional spar element is a uniaxial tension-compression element with three degrees of freedom at each node: translations in the nodal x, y, and z directions. This element is also capable of plastic deformation. The element is shown in Figure. 5.3(b).

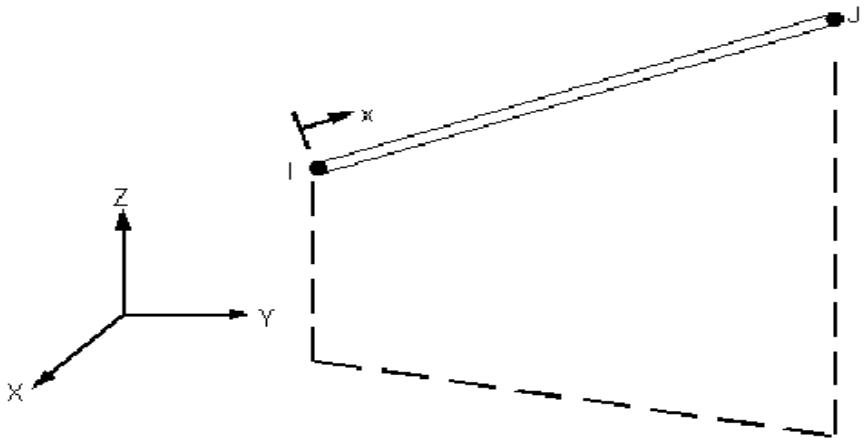

Figure 5.3 (b) LINK8 Element

5.6 MATERIAL MODELS

Problems involving material nonlinearity are considered in this thesis. It is assumed that displacements are small so that the geometric effects are small and hence the geometric effects can be neglected. However, depending upon the input given to the material models of concrete and steel in ANSYS, the response of the reinforced concrete column can be different. For the present analysis the following material models have been used.

5.6.1 STEEL REINFORCEMENT

The properties of reinforcing steel, unlike concrete, are generally not dependent on environmental conditions or time. Thus, the specification of a single stress-strain relation is sufficient to define the material properties needed in the analysis of reinforced concrete structures. For all practical purpose steel exhibits the same stress-strain curve in compression as in tension. For the present study, reinforcing steel has been considered as bilinear isotropic hardening.

Idealized elasto-plastic stress-strain behavior from a uniaxial tension test is shown in Figure 5.4, where initially the behavior is elastic until yield stress σ_y is reached. The elastic modulus is denoted by E. After yielding, the plastic phase begins with a slope of E_t, known as the tangent modulus.

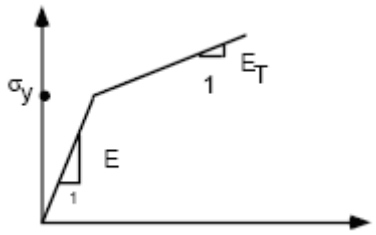

Figure 5.4 Idealized elasto-plastic stress-strain curve

5.6.2 CONCRETE MODELS

Development of a model for the behavior of concrete is a challenging task. Concrete is a quasi-brittle material and has different behavior in compression and tension. The tensile strength of the concrete is typically 10% of the compressive strength. In compression, the stress-strain curve for concrete is linearly elastic up to about 30% of the maximum compressive strength. After it reaches the maximum compressive strength, the curve descends in to a softening region, and eventually failure occurs at an ultimate strain. In tension, the stress-strain curve for concrete

is approximately linearly elastic up to the maximum tensile strength, beyond which, the concrete cracks and the strength decreases gradually to zero. The ANSYS program requires the uniaxial stress-strain relationship for concrete in compression. There are different models for concrete. Two of them are introduced here namely Multi crack model.

5.6.2.1 MULTI CRACK MODEL

Multi-linear Isotropic Hardening Stress-Strain Curve

The uniaxial behavior is described by a piece wise linear stress-strain curve, starting at the origin, with positive stress and strain values. The slope of the first segment of the curve must correspond to the elastic modulus of the material and no segment slope should be larger. No segment can have a slope less than zero. Numerical Expressions (Desayi and Krishnan [16]), Equation 39 and 40, have been used along with Equation 41 (Gere and Timoshenko [11]) to construct the multi-linear stress-strain curve for concrete in the study.

$$f = \frac{E_c \in}{1+\left(\frac{\in}{\in_0}\right)^2} \qquad \text{..……..... 39}$$

$$\in_0 = \frac{2 f_{ck}}{E_c} \qquad \text{……40}$$

$$E_c = \frac{f}{\in} \qquad \text{……41}$$

Where f - Stress at any strain

$\in$ - Strain at any stress

$\in_0$ - Strain at the ultimate compressive strength f_{ck}

Figure 5.5 shows the multi-linear isotropic stress-strain curve which is used for the present study.

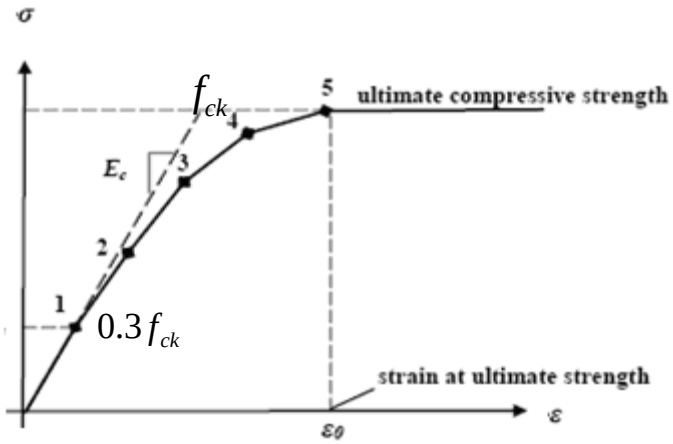

Figure 5.5 Multi-linear Isotropic stress-strain curve

The multi-linear isotropic stress-strain implementation requires the first point of the curve to be defined by the user. It must satisfy Hooke's Law. Stress strain properties of M 40 concrete has shown in Table 5.1.

Table 5.1 Stress-strain properties of M 40 concrete using multi crack model

Stress (MPa)	Strain (mm)
10	0.000321
15.20	0.0005
27.26	0.001
34.88	0.0015
40	0.002
40	0.0035

Chapter – 6

RESULTS AND DISCUSSION

Chapter 6

RESULTS AND DISCUSSION

6.1 RC COLUMN SUBJECTED TO BLAST LOADING

A ground floor column 6.4m high of a multi-storey building was analyzed in this study (see Fig. 6.1). The parameters considered were the concrete strength 40MPa for Normal strength column(NSC) and 80 MPa for High strength column(HSC) and stirrups spacing is 400mm for ordinary detailing and 100mm for special seismic detailing. It has been found that with increasing concrete compressive strength, the column size can be effectively reduced. In this case the column size was reduced from 500 x 900 mm for the NSC column down to 350 x 750 for the HSC column details given in Table 6.1, while the axial load capacities of the two columns are still the same.

The blast load was calculated based on data from the Oklahoma bombing report [13] with a stand off distance of 5 m. The simplified triangle shape of the blast load profile was used (see Fig.6.2). The duration of the positive phase of the blast is 1.3 milliseconds.

Table 6.1 Concrete grades and member size.

Column	Sizes	Grade of concrete(f_{ck})	Stirrups spacing	Detailing
NSC	500x900	40 N/mm^2	400mm	ordinary
NSC	500x900	40 N/mm^2	100mm	seismic
HSC	350x750	80 N/mm^2	400mm	ordinary
HSC	350x750	80 N/mm^2	100mm	seismic

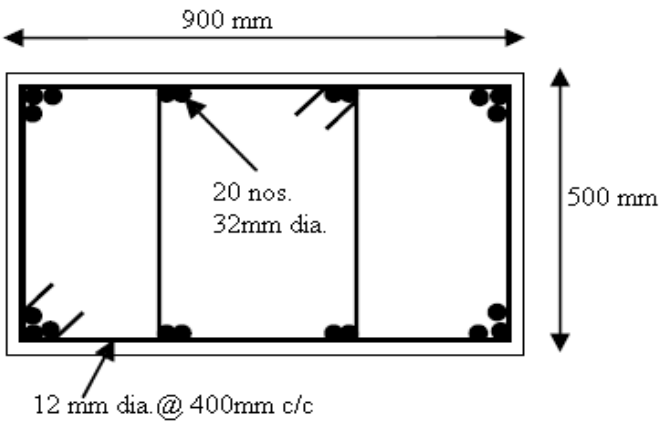

Figure 6.1 Cross section of the NSC column- ordinary detailing 400 mm stirrups spacing.

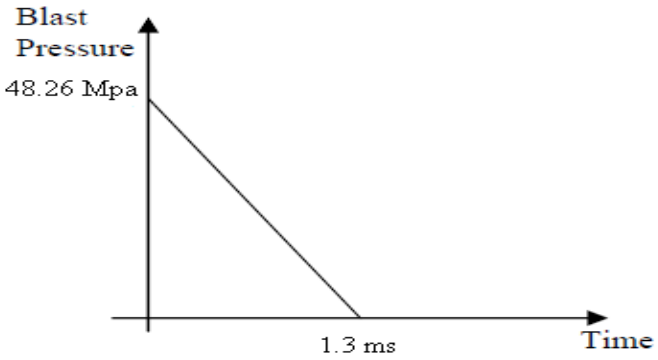

Figure 6.2 Blast loading

The duration of the positive phase of the blast is 1.3 milliseconds. The 3D model of the column was analysed using the ANSYS which takes into account both material nonlinearity and geometric nonlinearity. The effects of the blast loading were modelled in the dynamic analysis to obtain the deflection time history of the column.

Problem: Determine free-field blast wave parameters for a surface burst.

Procedure:

Step1. Select point of interest on the ground relative to the charge. Determine the charge weight, and ground distance R_G.

Step2. Apply a 20% safety factor to the charge weight.

Step3. Calculate scaled ground distance Z_G:

$$Z_G = \frac{R_G}{W^{1/3}}$$

Step 4. Determine free-field blast wave parameters from Figure A 1--7 for corresponding scaled ground distance Z_G:

Read:

Peak positive incident pressure *Pso*

Shock front velocity U_o

Scaled unit positive incident impulse $i_s/W^{1/3}$

Scaled positive phrase duration $t_o/W^{1/3}$

Scaled arrival time $t_A/W^{1/3}$

Multiply scaled values by $W^{1/3}$ to obtain absolute values.

Example:-

Required: Free-field blast wave parameters P_{so}, U_o, i_s, t_o, t_A for a surface burst of W=1814 Kg=3990.8 lbs at a distance of R_h= 5m = 16.40ft

1. **For height h = 0 m,**

Solution:

Step 1: Given: Charge weight = 1814Kg = 3990.8 lb, Rh = 16.40 ft

Step 2. W = 1.20 (3990.5) = 4788.5 lbs

Step 3. For point of interest:

$$Z_G = \frac{R_G}{W^{1/3}} = \frac{16.40}{4788.5^{1/3}} = 0.973\, ft/lb^{1/3}$$

Step 4. Determine blast wave parameters from Fig.A 1--7 for

Z_G = 0.973 ft/lb1/3

P_r = 7000psi = 7 Ksi =7 x 6.895 = 48.265 Mpa

P_{so} = 850 psi = 0.880 Ksi =0.850 x 6.895 = 5.86 Mpa

$\frac{i_s}{W^{1/3}} = 16 psi - ms/lb^{1/3}$; i_s= 16(4788.5)$^{1/3}$= 269.68 psi-ms = 1.86Mpa-ms

$\frac{i_r}{W^{1/3}} = 220 psi - ms/lb^{1/3}$; i_r=220(4788.5)$^{1/3}$ = 3708.14psi-ms = 25.56Mpa-ms

$\frac{t_A}{W^{1/3}} = 0.08 ms/lb^{1/3}$; t_A= 0.08(4788.5)$^{1/3}$ = 1.34 ms

$\frac{t_o}{W^{1/3}} = 0.19 ms/lb^{1/3}$; t_o = 0.19 (4788.5)$^{1/3}$ = 3.2 ms

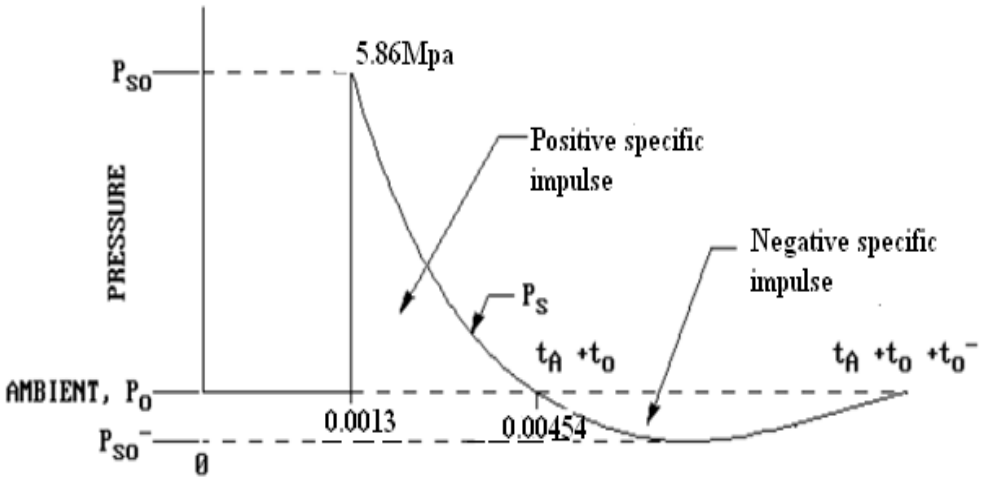

Figure 6.3 Free-field pressure –time variation for height= 0m.

2. **For height h = 6.4m = 21 ft,**

Solution:

Step 1: Given: Charge weight = 1814Kg = 3990.8 lb, Rh = $\sqrt{16.4^2 + 21^2}$ = 26.65 ft.

Angle of incident (α) = $\tan^{-1}\left(\frac{26.65}{16.40}\right) = 58.39^o > 45^o$

Angle of incident (α) = 45°

Step 2. W = 1.20 (3990.5) = 4788.5 lbs

Step 3. For point of interest:

$$Z_G = \frac{R_G}{W^{1/3}} = \frac{26.65}{4788.5^{1/3}} = 1.582\, ft/lb^{1/3}$$

Step 4. Determine blast wave parameters from Fig.A 1--7 for

Z_G = 1.582 ft/lb1/3

P_r = 2800psi = 2.8 Ksi = 2.8 x 6.895 = 19.306 Mpa

P_{so} = 390 psi = 0.39 Ksi = 0.39 x 6.895 = 2.690 Mpa

$\frac{i_s}{W^{1/3}} = 18\, psi - ms/lb^{1/3}$; i_s= 18(4788.5)$^{1/3}$= 303.4 psi-ms = 2.10Mpa-ms

$\frac{i_r}{W^{1/3}} = 120\, psi - ms/lb^{1/3}$; i_r= 120(4788.5)$^{1/3}$ = 2022.62 psi-ms = 13.95Mpa-ms

$\frac{t_A}{W^{1/3}} = 0.18 ms/lb^{1/3}$; t_A= 0.18(4788.5)$^{1/3}$ = 3.04 ms

$\frac{t_o}{W^{1/3}} = 0.4 ms/lb^{1/3}$; t_o = 0.4 (4788.5)$^{1/3}$ = 6.75 ms

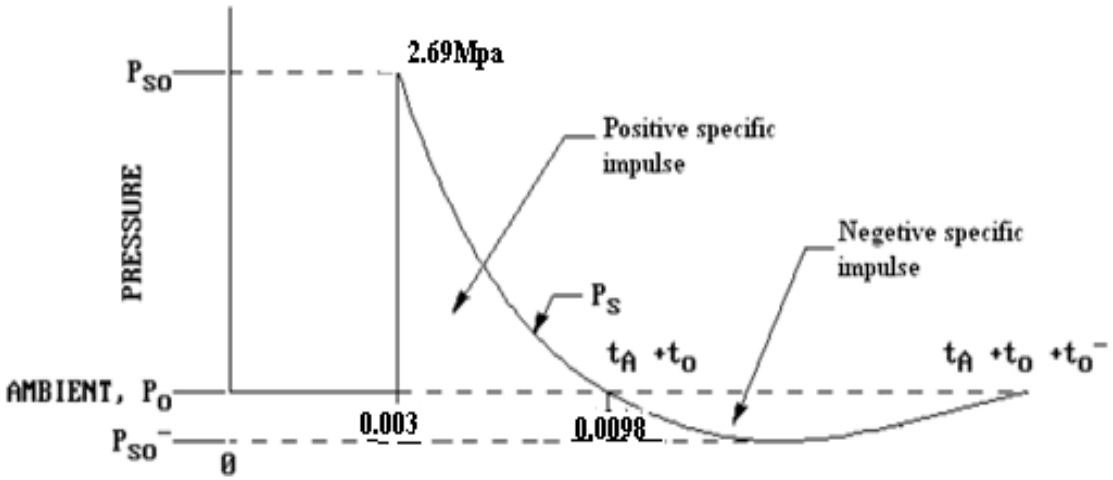

Figure 6.4 Free-field pressure –time variation for height = 6.4

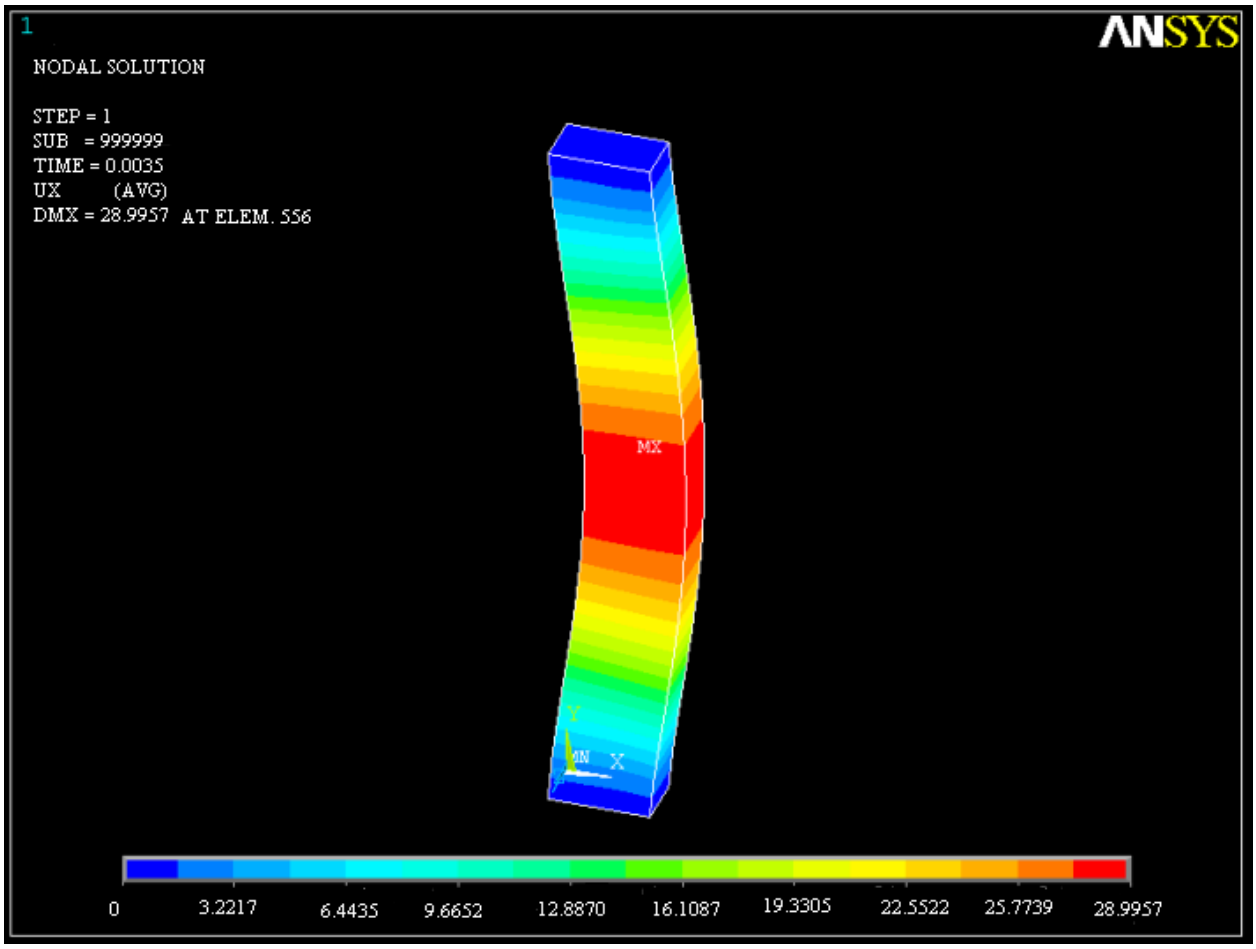

Figure 6.5. 3D model of the column using ANSYS.

6.2 RESULTS

The lateral deflection at mid point versus time history of two columns made of NSC and HSC are shown in Figs.6.6 and 6.7. The graphs clearly show the lateral resistance of the columns. It can be seen that under this close-range bomb blast both columns failed in shear. However, the 80MPa columns with reduced cross section have a higher lateral deflection.

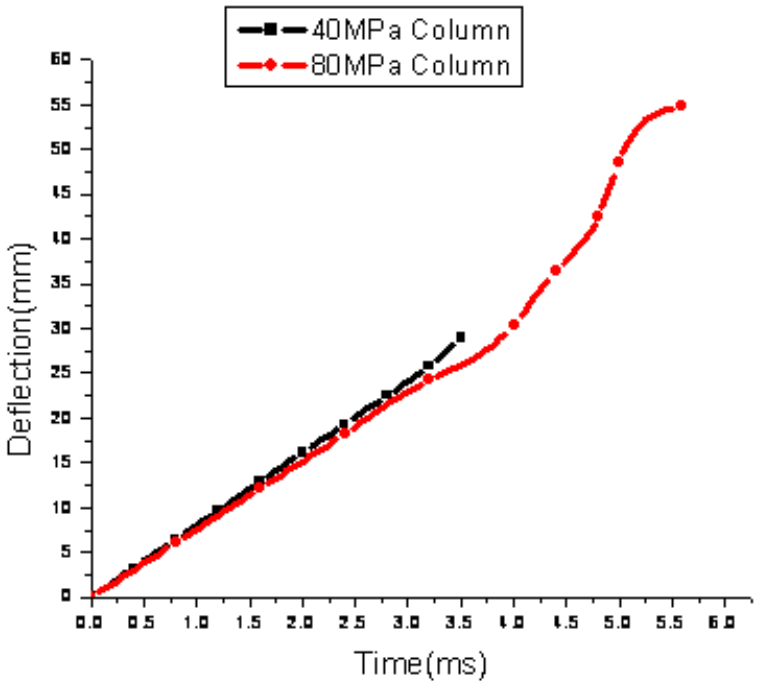

Figure 6.6, Lateral Deflection – Time history at mid point of column with 400 mm stirrups spacing.

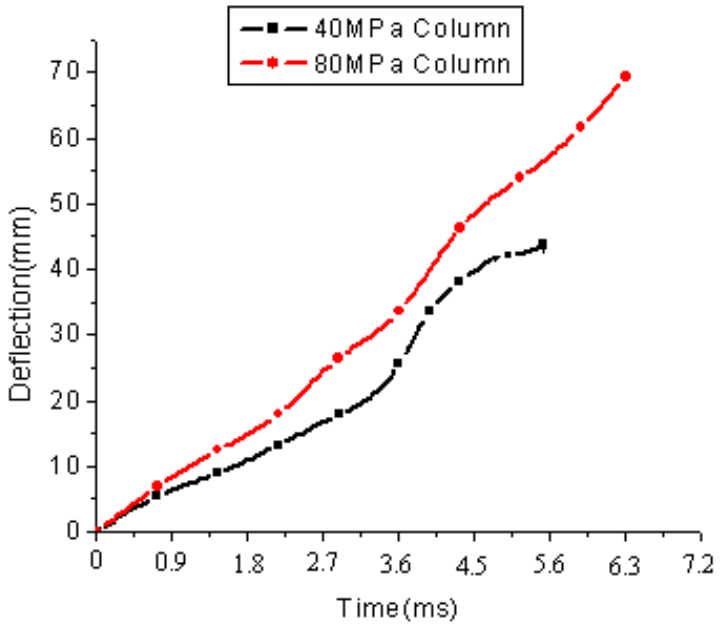

Figure 6.7, Lateral Deflection – Time history at mid point of column with 100 mm stirrups spacing

It can be seen from Figs.6.6 and 6.7 that the effect of shear reinforcement is also significant. The ultimate lateral displacements at failure increase from 54 mm (400 mm stirrups spacing) to 69 mm (100 mm stirrups spacing) for the HSC column. Those values for the NSC column are 29mm (400 mm stirrups spacing) and 43 mm (100 mm stirrups spacing), respectively.

Table 6.2 Comparison of the lateral deflection at mid point of HSC and NSC columns.

Column	Stirrups spacing	Lateral deflection at mid point	
		Using LSDYNA [24]	Using ANSYS
NSC	400 mm c/c	20 mm	29 mm
NSC	100 mm c/c	32 mm	43 mm
HSC	400 mm c/c	45 mm	54 mm
HSC	100 mm c/c	63 mm	69 mm

Chapter – 7

CONCLUSIONS AND FUTURE SCOPE OF STUDY

Chapter 7

CONCLUSIONS AND FUTURE SCOPE OF STUDY

7.1CONCLUSIONS

Based on the studies available in the literature, the ultimate objective is to make available the procedure for calculating the blast loads on the structures with or without the openings and frame structures. Also to study the dynamic properties of reinforcing steel and concrete under high strain rates typically produce by the blast loads. From this part of the study, an understanding of how reinforced concrete columns respond to blast loads was obtained.

The following observations and conclusions are drawn from this study

1. The finite element analysis revealed that, for axially loaded columns, there exists a critical lateral blast impulse. Any applied blast impulse above this value will result in the collapsing of the column before the allowable beam deflection criterion is reached.
2. The column response to non-uniform blast loads was shown to be significantly influenced by higher vibration modes. This was especially true for the unsymmetrical blast loads.
3. The comparison between the normal strength column and the higher strength column showed that the critical impulse for the higher strength column case is significantly higher. This increase can be attributed to the added stiffness.
4. The surfaces of the structure subjected to the direct blast pressures can not be protected; it can, however, be designed to resist the blast pressures by increasing the stand-off distance from the point of burst.
5. For high-risks facilities such as public and commercial tall buildings, design considerations against extreme events (bomb blast, high velocity impact) are very

important. It is recommended that guidelines on abnormal load cases and provisions on progressive collapse prevention should be included in the current Building Regulations and Design Standards. Requirements on ductility levels also help to improve the building performance under severe load conditions.

7.2 FUTURE SCOPE OF STUDY

1. Cases in which the axial load does not remain constant during the column response time are possible. These include situations where the bomb is located within the structure and the blast excites the girders connected to the column. The effect of this time-varying axial load should be studied.
2. Cases should be studied when the explosions within a structure can cause failure of interior girders, beams and floor slabs.
3. Tests and evaluation of connections under direct blast loads.
4. Tests and design recommendations for base plate configurations and designs to resist direct shear failure at column bases.

References

REFERENCES

1. A. Khadid et al. (2007), " Blast loaded stiffened plates" Journal of Engineering and Applied Sciences,Vol. 2(2) pp. 456-461.
2. A.K. Pandey et al. (2006) "Non-linear response of reinforced concrete containment structure under blast loading" Nuclear Engineering and design 236. pp.993-1002.
3. Alexander M. Remennikov, (2003) "A review of methods for predicting bomb blast effects on buildings", Journal of battlefield technology, vol 6, no 3. pp 155-161.
4. American Society for Civil Engineers 7-02 (1997), "Combination of Loads",pp 239-244.
5. ANSYS Theory manual, version 5.6, 2000.
6. Biggs, J.M. (1964), "Introduction to Structural Dynamics", McGraw-Hill, New York.
7. Dannis M. McCann, Steven J. Smith (2007), "Resistance Design of Reinforced Concrete Structures", STRUCTURE magazine, pp 22-27, April issue.
8. Demeter G. Fertis (1973), "Dynamics and Vibration of Structures", A Wiley-Interscience publication, pp. 343-434.
9. D.L. Grote et al. (2001), "Dynamic behaviour of concrete at high strain rates and pressures", Journal of Impact Engineering, Vol. 25, Pergamon Press, NewYork, pp. 869-886,
10. IS 456:2000 Indian Standard Plain and Reinforced Concrete Code of Practice.
11. J.M. Dewey (1971), "The Properties of Blast Waves Obtained from an analysisof the particle trajectories", Proc. R. Soc. Lond. A.314, pp. 275-299.
12. J.M. Gere and S.P. Timoshenko (1997.), "Mechanics of materials", PWS publishing company, Buston, Massachusetts,

13. Kirk A. Marchand, Farid Alfawakhiri (2005), “Blast and Progressive Collapse” fact for Steel Buildings, USA.

14. M. V. Dharaneepathy et al. (1995),“Critical distance for blast resistance design”, computer and structure Vol. 54, No.4.pp.587-595.

15. Nelson Lam et al. (2004), “Response Spectrum Solutions for Blast Loading”, Journal of Structural Engineering, pp 28-44.

16. P. Desayi and S. Krishnan (1964), “ Equation for the stress-strain curve of concrete”. Journal of the American Concrete Institute, 61, pp 345-350.

17. S.Unnikrishna Pillai and Devdas Menon(2003), “Reinforced Concrete Design”, Tata McGraw-Hill.

18. Ronald L. Shope (2006), “Response of wide flange steel columns subjected to constant axial load and lateral blast load”. Civil Engineering Department, Blacksburg, Virginia.

19.Schmidt, Jon A. (2003), “Structural Design for External Terrorist Bomb Attacks”, STRUCTURER magazine, March issue.

20. S.Unnikrishna Pillai and Devdas Menon (2003) , “Reinforced Concrete Design”, Tata McGraw-Hill, pp 121-196.

21. T. A. Rose et al. (2006), “The interaction of oblique blast waves with buildings”, Published online: 23 August 06 © Springer-Verlag, pp 35-44.

22. T. Borvik et al.(2009) “Response of structures to planar blast loads – A finite element engineering approach” Computers and Structures 87, pp 507–520,

23. TM 5-1300(UFC 3-340-02) U.S. Army Corps of Engineers (1990), “Structures to Resist the Effects of Accidental Explosions”, U.S. Army Corps of Engineers, Washington, D.C., (also Navy NAVFAC P200-397 or Air Force AFR 88-22).

24. T. Ngo, P. Mendis, A. Gupta & J. Ramsay, " Blast Loading and Blast Effects on structure", The University of Melbourne, Australia, 2007.

25. Wai-Fah Chen and Atef F. Saleeb (1994), "Constitutive Equations for Engineering Materials-Volume 1: Elasticity and Modeling", Elsevier Science B.V.

APPENDIX

APPENDIX A

Figure A1. Positive Phase Shock Wave Parameter for a Spherical TNT Explosion in Free Air.

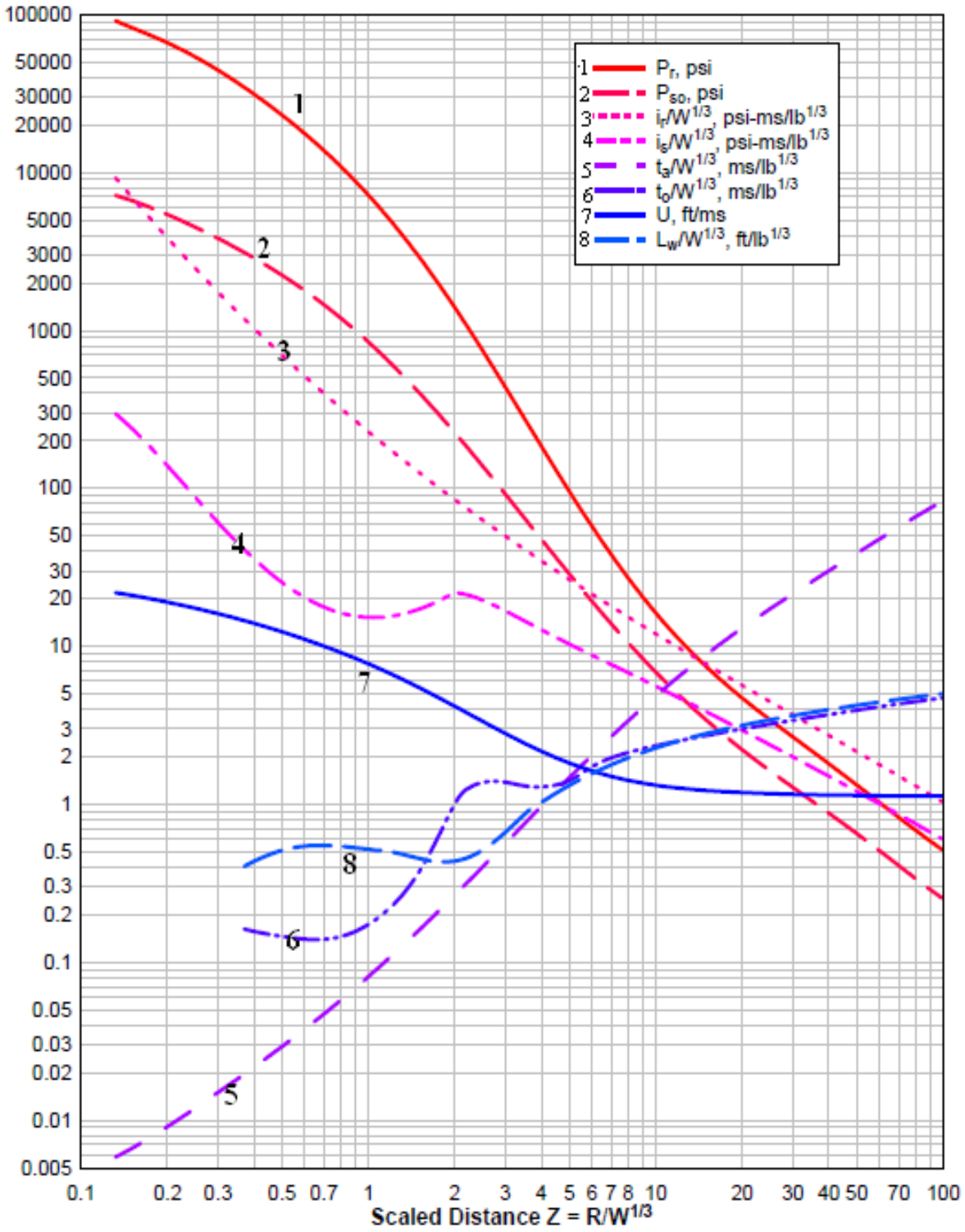

Figure A2. Negative Phase Shock Wave Parameter for a Spherical TNT Explosion in Free Air.

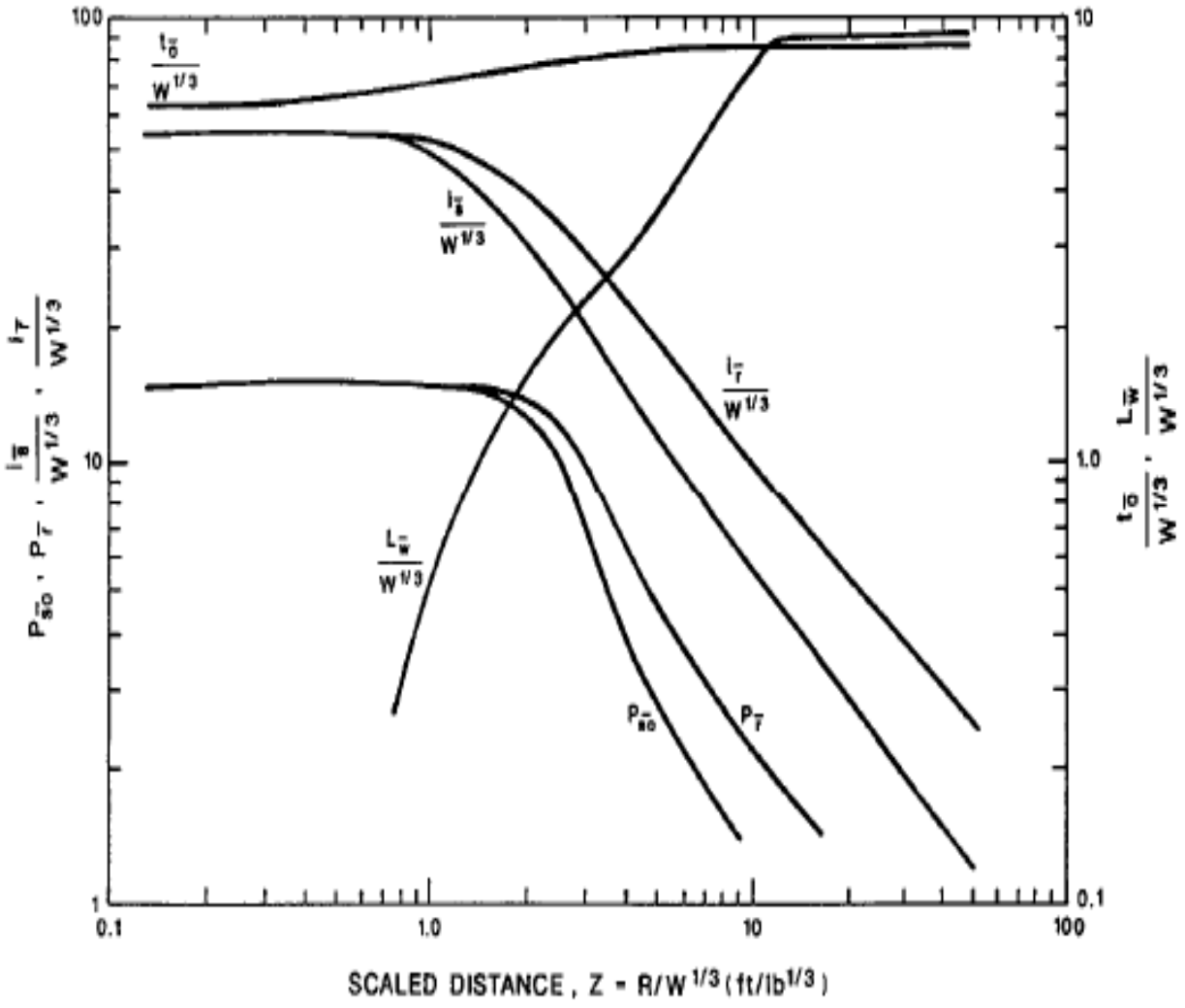

Figure A3. Variation of Reflected Pressure as a Function of Angle of Incidence.

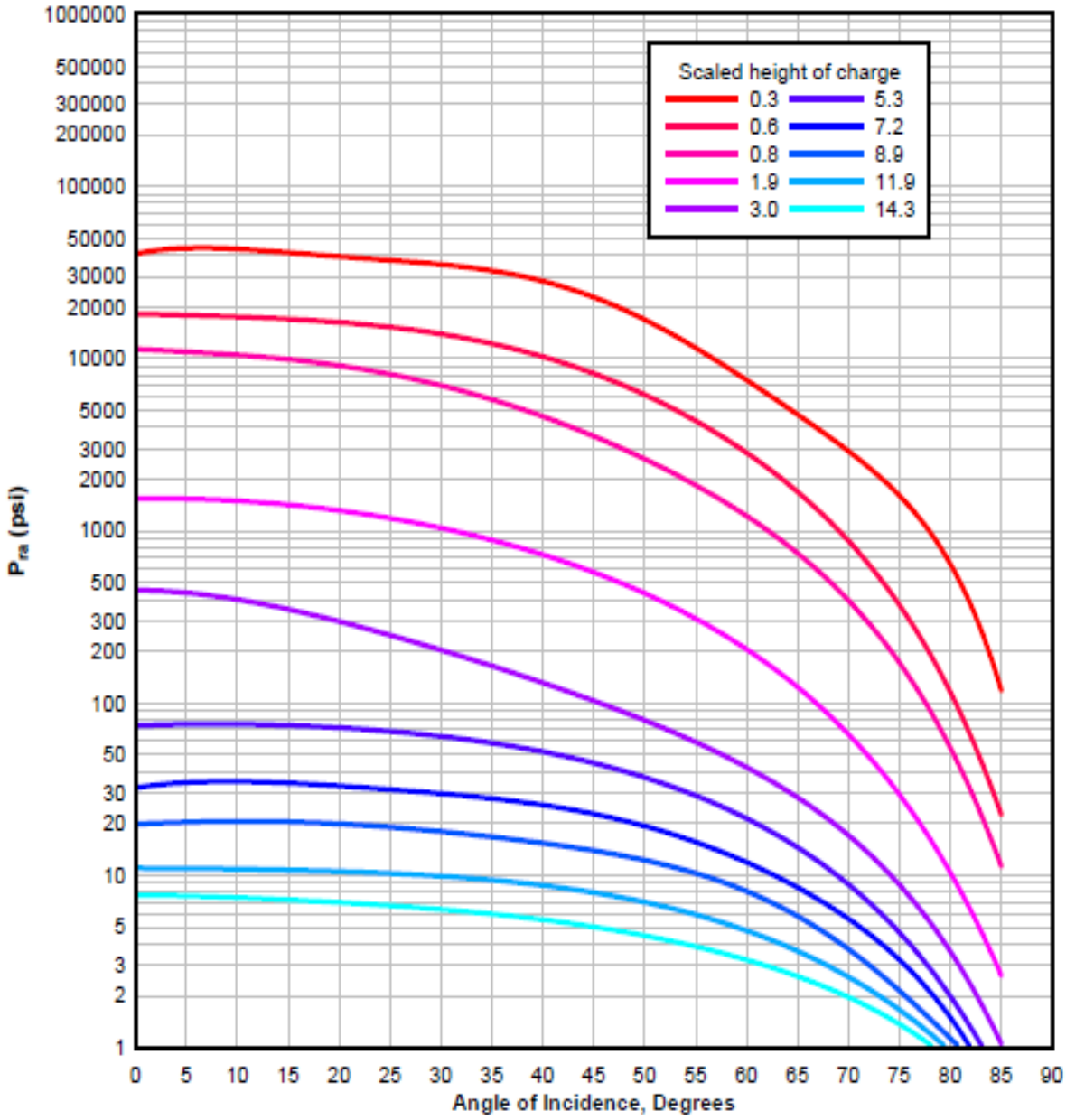

Figure A4. Variation of Scaled Reflected Impulse as a Function of Incidence

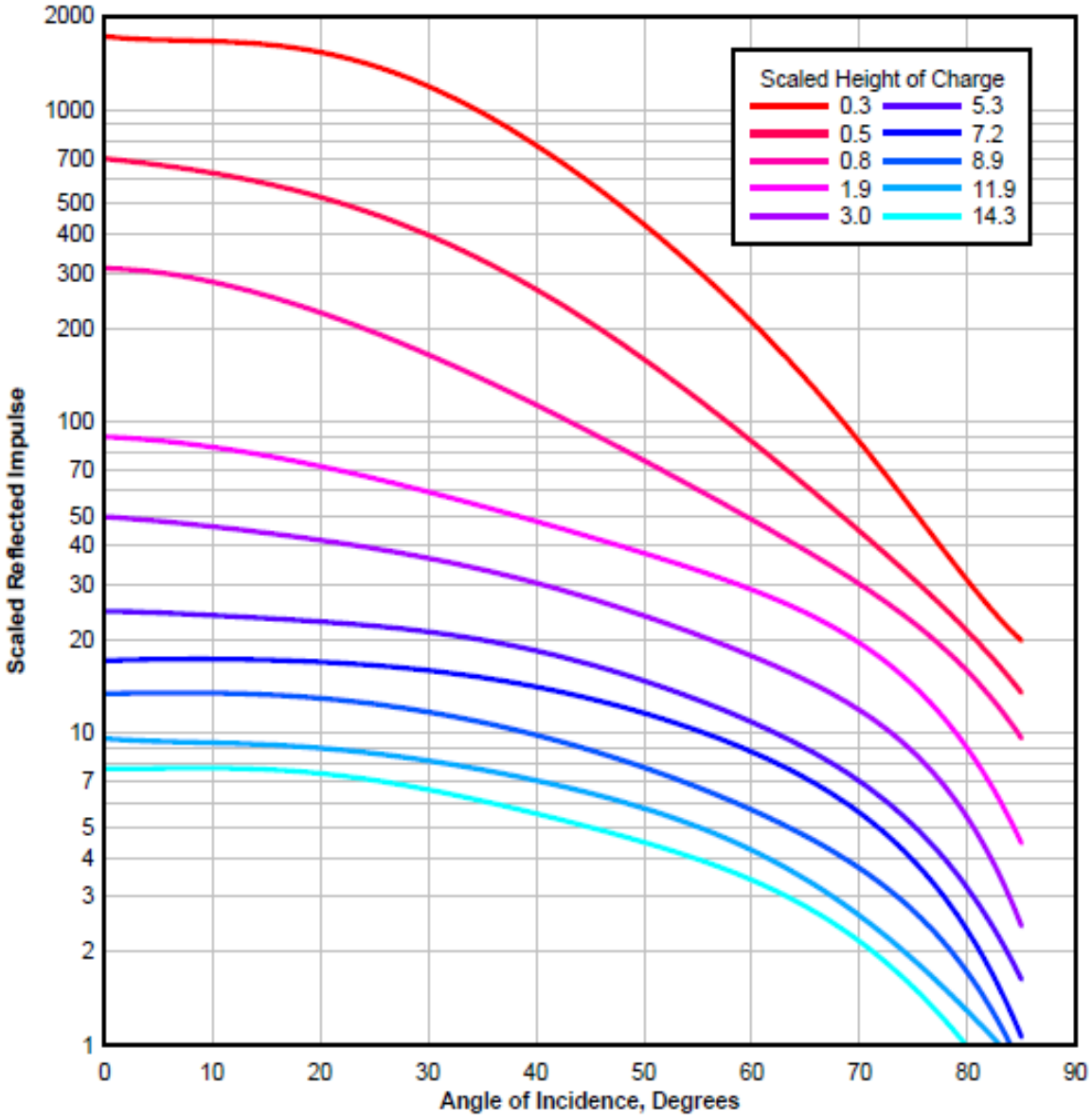

Figure A5. Peak Incident Pressure versus the Ratio of Normal Reflected Pressure/ Incidence Pressure for a Free Air Burst.

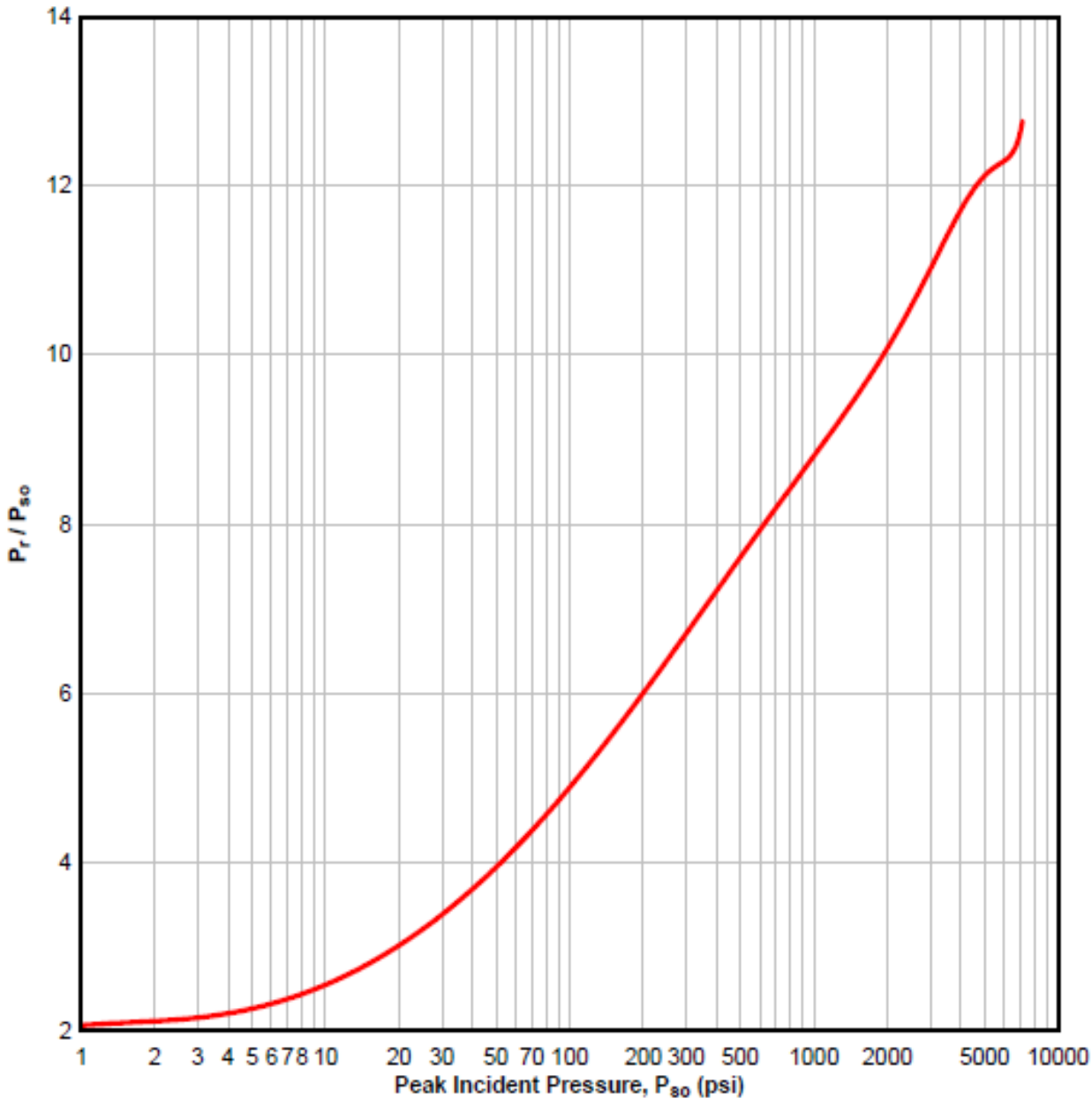

Figure A6. Peak Incident Pressure versus Peak Dynamic Pressure, Density of Air Behind the Shock Front, and Particle Velocity.

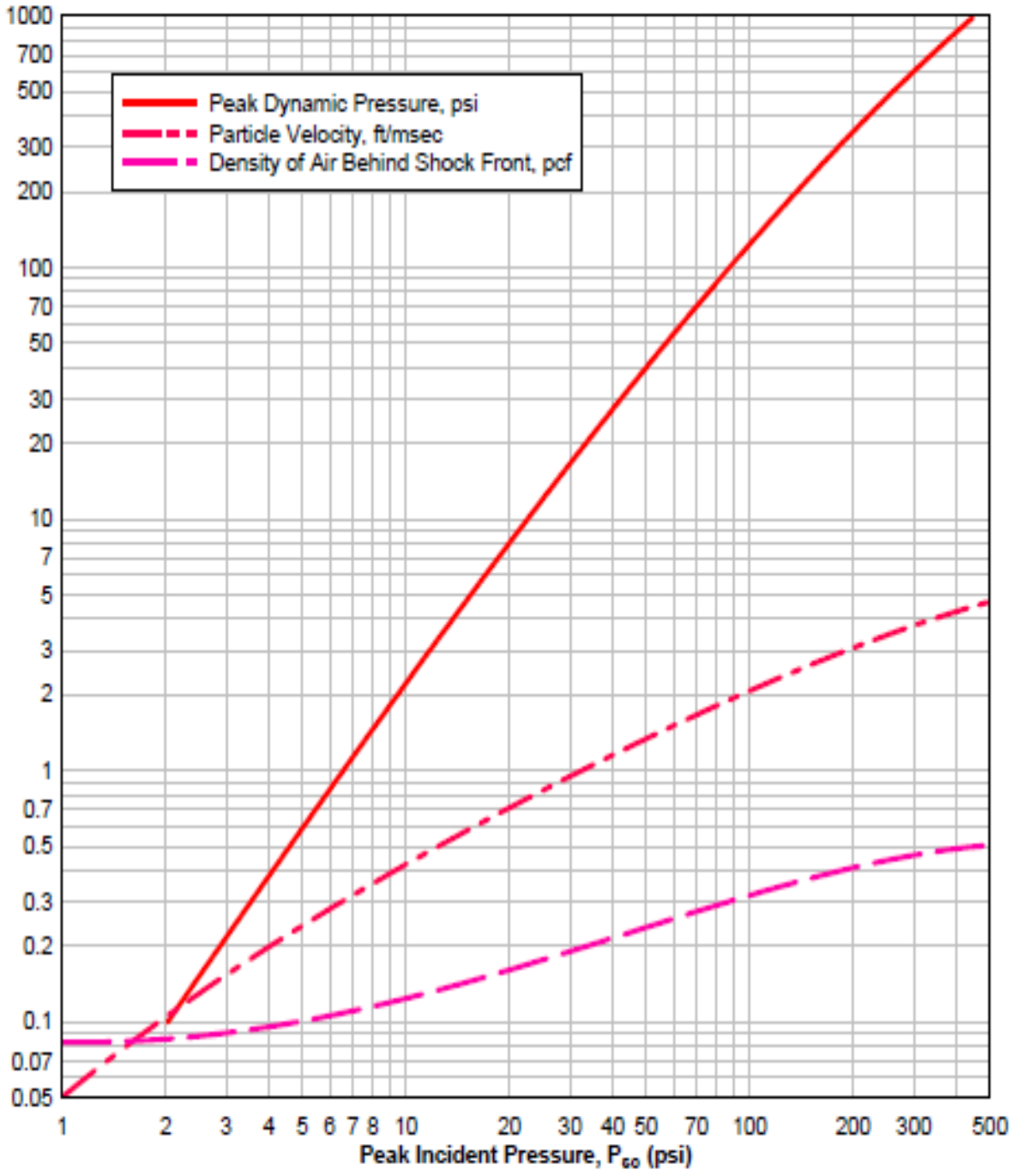

Figure A7. Positive Phase Shock Wave Parameters for a Hemispherical TNT Explosion on The surface.

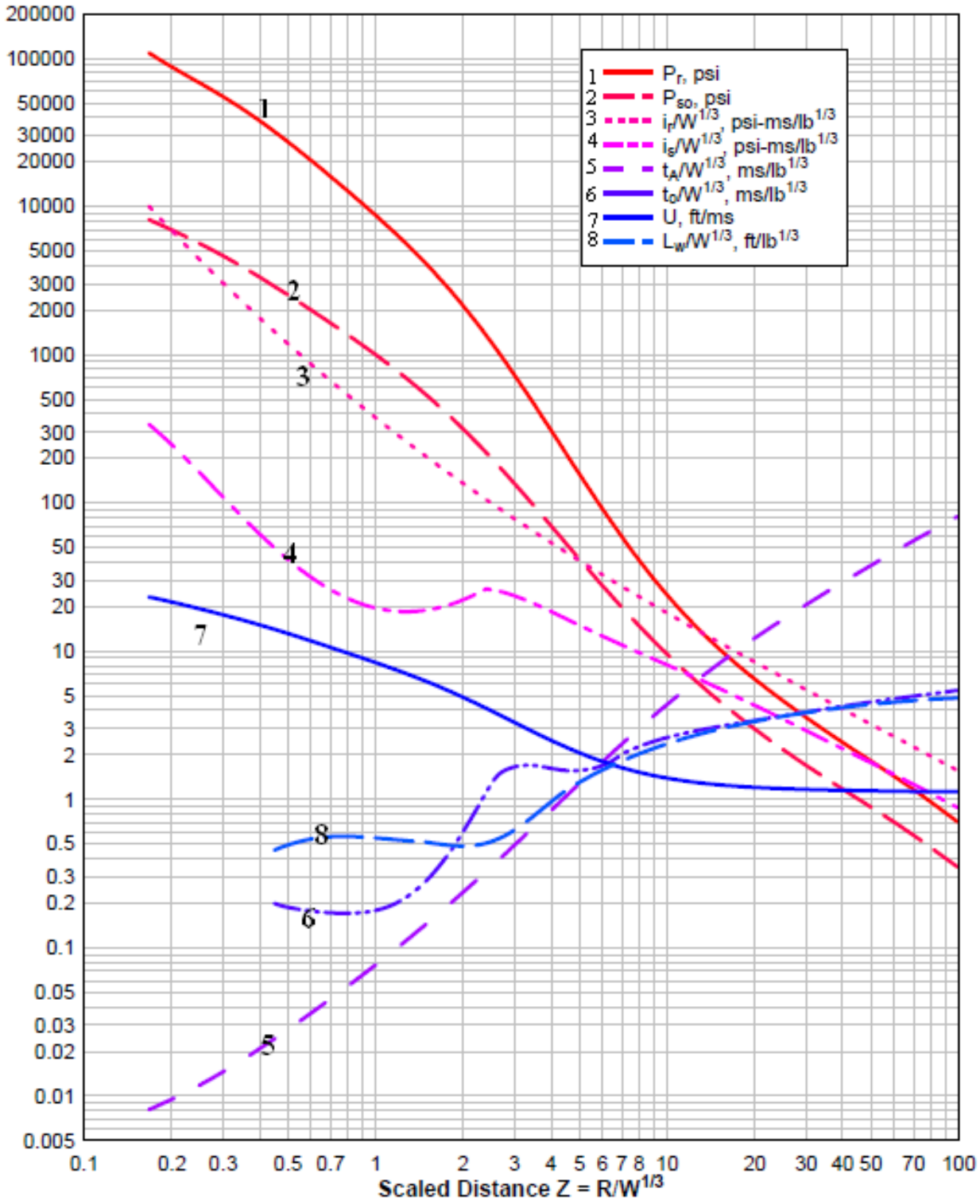

Figure A8. 3D finite element model of simple RC column in ANSYS.

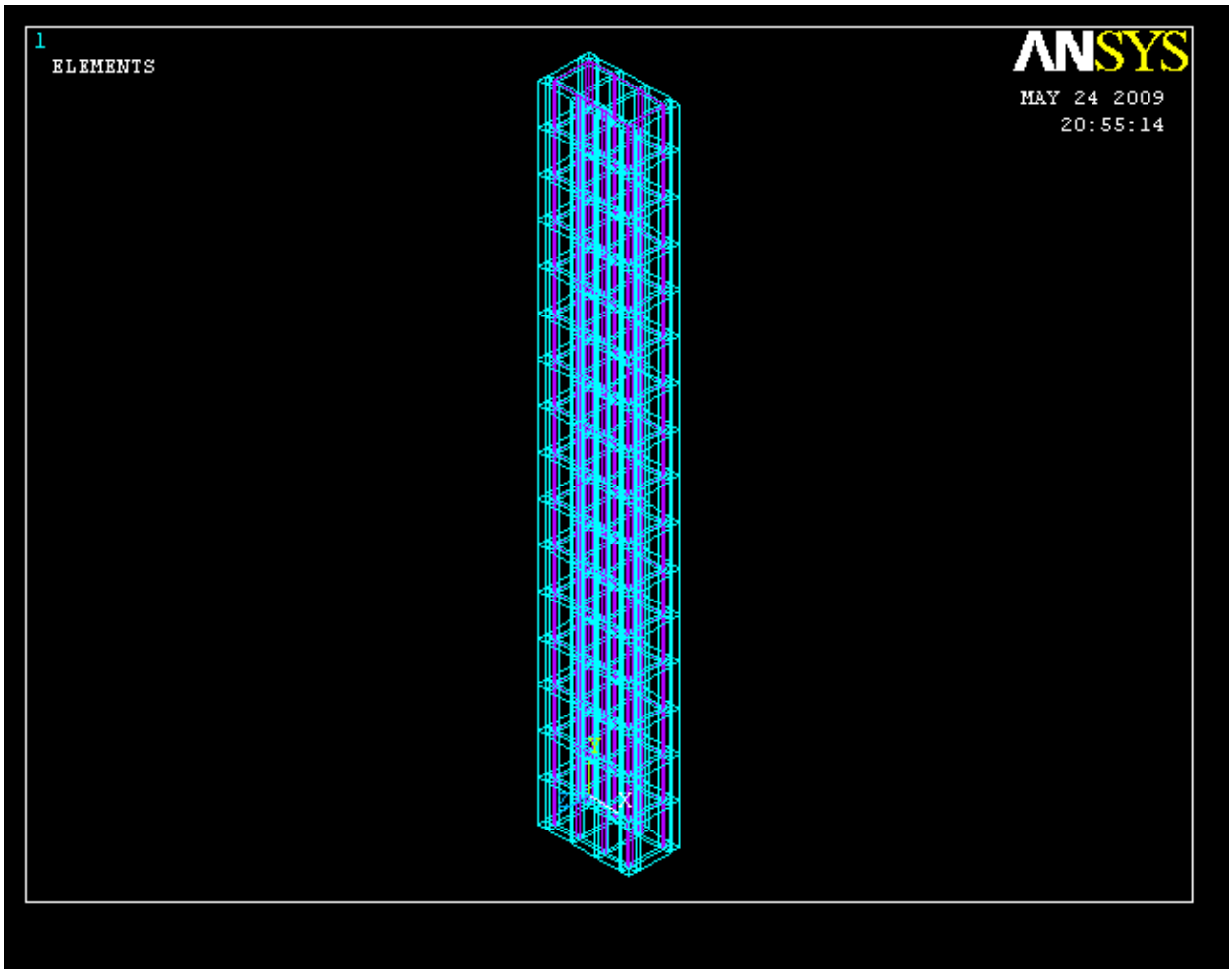

Figure A 9. 3D finite element model of simple RC column with axial load and blast pressure.